Natural Killer T Cells Are Involved in Adipose Tissues Inflammation and Glucose Intolerance in Diet-Induced Obese Mice

Kazue Ohmura; Naoki Ishimori; Yoshinori Ohmura; Satoshi Tokuhara; Atsushi Nozawa; Shunpei Horii; Yasuhiro Andoh; Satoshi Fujii; Kazuya Iwabuchi; Kazunori Onoé; Hiroyuki Tsutsui

Background—Macrophage and lymphocyte infiltration in adipose tissue may contribute to the pathogenesis of obesity-mediated metabolic disorders. Natural killer T (NKT) cells, which integrate proinflammatory cytokines, have been demonstrated in the atherosclerotic lesions and in visceral adipose tissue.

Objective—To determine whether NKT cells are involved in glucose intolerance and adipose tissue inflammation in diet-induced obese mice.

Methods and Results—Male β_2-microglobulin knockout (KO) mice lacking NKT cells and C57BL/6J (wild-type) mice were fed with a high-fat diet (HFD) for 13 weeks. Body weight and visceral obesity were comparable between wild-type and KO mice. However, macrophage infiltration was reduced in adipose tissue and glucose intolerance was significantly ameliorated in KO mice. To further confirm that NKT cells are involved in these abnormalities, α-galactosylceramide, 0.1 μg/g body weight, which specifically activates NKT cells, was administered after 13 weeks of HFD feeding. α-Galactosylceramide significantly exacerbated glucose intolerance and macrophage infiltration as well as cytokine gene expression in adipose tissue.

Conclusion—NKT cells play a crucial role in the development of adipose tissue inflammation and glucose intolerance in diet-induced obesity. **(*Arterioscler Thromb Vasc Biol.* 2010;30:193-199.)**

Key Words: obesity ■ natural killer T cells ■ macrophages ■ visceral adipose tissues ■ glucose intolerance

Obesity, specifically visceral obesity, increases the risk for metabolic disorders, such as type 2 diabetes mellitus, dyslipidemia, and hypertension as well as atherosclerotic cardiovascular diseases. Previous studies have demonstrated that the accumulation of macrophages within adipose tissue is well documented in obese individuals and that adipose tissue inflammation plays an important role in the pathogenesis of these metabolic disorders.[1,2] Macrophages are attracted by chemokines, such as monocyte chemoattractant protein 1 (MCP-1), and contribute to local inflammation through the release of other inflammatory cytokines, such as tumor necrosis factor (TNF) α. In high-fat diet (HFD)-fed obese mice, it has been shown that infiltration of macrophages into adipose tissue coincides with the occurrence of obesity-mediated metabolic disorders.[2] The important role of adipose tissue macrophages in the pathogenesis of metabolic disorders has further been supported by recent data in C-C motif chemokine receptor 2 (CCR2)–deficient mice.[3] The CCR2$^{-/-}$ mice exhibited a reduction in adipose tissue macrophages in association with an improvement of glucose homeostasis and insulin sensitivity. However, the abolished monocyte and macrophage recruitment into peripheral tissue via interaction with MCP-1 could not completely inhibit HFD-mediated metabolic disorders, suggesting that other inflammatory cells may play a role in this context. Wu et al[4] and Rocha et al[5] demonstrated that CD3-positive T lymphocytes are present in human adipose tissue; and regulated upon activation, normal T cell expressed secreted (RANTES), a T-cell–specific chemokine, and its respective receptor CCR5 are expressed in adipose tissue from obese patients. However, the role of other types of lymphocytes in adipose tissue inflammation is largely unexplored.

See accompanying article on page 135

Natural killer T (NKT) cells are innatelike T lymphocytes that recognize glycolipid antigens and are capable of rapidly producing a mixture of T-helper type 1 (T_H1) and T_H2 cytokines, such as interferon (IFN) γ and interleukin (IL) 4 in shaping subsequent adaptive immune responses.[6] Thus, NKT cells can function as a bridge between the innate and adaptive

Received January 29, 2009; revision accepted October 19, 2009.

From the Department of Cardiovascular Medicine, Hokkaido University Graduate School of Medicine, Sapporo, Japan (K.O., N.I., Y.O., S.T., A.N., S.H., Y.A., and H.T.); the Department of Molecular and Cellular Pathobiology and Therapeutics, Nagoya City University Graduate School of Pharmaceutical Sciences, Nagoya, Japan (S.F.); Division of Immunobiology, Institute for Genetic Medicine, Hokkaido University, Sapporo, Japan (K.I. and K.O.).

Correspondence to Naoki Ishimori, MD, PhD, Department of Cardiovascular Medicine, Hokkaido University Graduate School of Medicine, Kita-15, Nishi-7, Kita-ku, Sapporo 060-8638, Japan. E-mail ishimori@med.hokudai.ac.jp

Arterioscler Thromb Vasc Biol **is available at http://atvb.ahajournals.org** **DOI: 10.1161/ATVBAHA.109.198614**

immune systems. Caspar-Bauguil et al[7] have reported the presence of significant levels of NKT cells in the stroma-vascular fraction of white adipose tissue by cytofluorometric analysis. However, they have not determined whether NKT cells are involved in adipose tissue inflammation and the development of metabolic disorders, including glucose intolerance in HFD-induced obesity.

Some of the processes involved in adipose tissue inflammation resemble inflammatory processes in atherogenesis.[8] Inflammation during the development of an atherosclerotic lesion is also characterized by monocyte/macrophage and lymphocyte infiltration.[8] These lymphocytes are mainly CD4-positive lymphocytes that express proinflammatory T_H1 cytokines, such as IFN-γ, and orchestrate the inflammatory response in the vascular wall by activating other cells. Previous studies,[9,10] including our own studies, demonstrated that NKT cells were present in atherosclerotic lesions and are critically important in atherogenesis. These findings suggest that NKT cells can also be involved in inflammation within adipose tissue. However, to date, it remains unclear whether NKT cells play a similar role in adipose tissue inflammation.

In the present study, we determined whether NKT cells are involved in HFD-induced glucose intolerance and adipose tissue inflammation by using β_2 microglobulin knockout (KO) mice lacking NKT cells. Moreover, we further examined the effects of NKT cell activation by α-galactosylceramide (αGC), a specific activator for NKT cells,[11] on glucose intolerance and adipose tissue inflammation in HFD-induced obese mice.

Methods

Expanded materials and methods are available in the supplemental files (available online at http://atvb.ahajournals.org).

Experiment 1: The Effects of NKT Cell Depletion on Metabolic Disorders

Male wild-type (WT) (Charles River Japan, Inc, Yokohama, Japan) and KO mice, which lack NKT and T cells on the C57BL/6 background (The Jackson Laboratory, Bar Harbor, Maine), aged 8 weeks, were fed with a standard diet (SD) (WT-SD, n=10; and KO-SD, n=5) or an HFD containing 21% fat and 0.15% cholesterol (WT-HFD, n=10; and KO-HFD, n=14) for 13 weeks. Animals were metabolically phenotyped, including an intraperitoneal glucose tolerance test (ipGTT). Other WT mice, aged 8 weeks, were fed with an SD (n=15) or an HFD (n=15) for 2, 4, or 6 weeks. Afterward, animals underwent euthanasia and organs, including visceral adipose tissue, were dissected.

Experiment 2: The Effects of NKT Cell Activation on Metabolic Disorders

After feeding male WT and KO mice, aged 8 weeks, with an HFD for 13 weeks, phosphate-buffered saline (PBS) (WT-PBS, n=5; and KO-PBS, n=5) or αGC, 0.1 μg/g body weight (Kirin Brewery Company, Ltd, Tokyo, Japan) (WT-αGC, n=5; and KO-αGC, n=5), was injected intraperitoneally. After 8 to 9 days, ipGTT was performed and visceral adipose tissues were dissected. Other WT mice, aged 8 weeks, were injected using PBS (n=9) or αGC, 0.1 μg/g body weight (n=11) intraperitoneally and organs, including visceral adipose tissues, were dissected 1, 4, and 7 days after the injection.

The animal care and procedures for the experiments were approved by the Committee of Hokkaido University Graduate School of Medicine on Animal Experimentation.

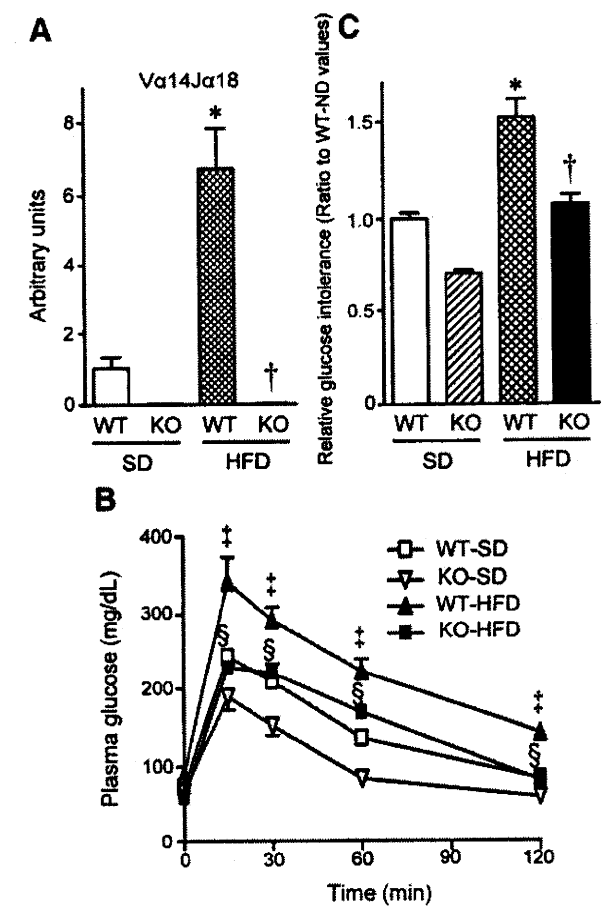

Figure 1. A, Vα14/Jα18 gene expression, an index of natural killer T (NKT) cells, of visceral adipose tissues in experiment 1. B, Plasma glucose concentrations. C, Area under the curve (AUC) values during the intraperitoneal glucose tolerance test (ipGTT). *$P<0.01$ vs wild type (WT)–standard diet (SD), †$P<0.01$ vs WT–high-fat diet (HFD), ‡$P<0.01$ vs WT-SD at each time, and §$P<0.01$ vs WT-HFD at each time.

Results

NKT Cell Depletion Ameliorates Metabolic Disorders in HFD-Fed Mice

To characterize the role of NKT cells in the pathogenesis of HFD-induced glucose intolerance and visceral adipose tissue inflammation, WT and KO mice were fed with either SD or HFD for 13 weeks.

The quantification of NKT cells by Vα14/Jα18 gene expression confirmed that NKT cell infiltration was significantly enhanced in adipose tissue from HFD mice and, more important, was completely abolished in KO groups (Figure 1A).

An HFD did not affect fasting plasma levels of glucose, insulin, and homeostasis model assessment of insulin resistance (HOMA-IR) in WT-HFD and KO-HFD compared with WT-SD (Table 1). However, plasma glucose levels during ipGTT were significantly increased in WT-HFD than in WT-SD, and these values were significantly lower in KO-HFD (Figure 1B). The area under the curve values of plasma glucose levels during the ipGTT were significantly increased in WT-HFD, and this increase was attenuated in KO-HFD to the WT-SD levels (Figure 1C). These results demonstrated that glucose intolerance seen in HFD-fed mice was significantly

Table. Animal Characteristics in Experiment 1

	Animal Group			
Characteristic	WT-SD (n=10)	KO-SD (n=5)	WT-HFD (n=10)	KO-HFD (n=14)
Body weight, g	29.4 (0.5)	29.4 (1.4)	33.2 (0.6)*	31.4 (0.7)
Blood chemistry results				
Fasting plasma glucose level, mg/dL	78 (8)	50 (8)†	82 (8)	55 (4)‡
Insulin level, ng/mL	0.49 (0.09)	0.27 (0.06)	0.77 (0.22)	0.90 (0.13)
HOMA-IR level	2.10 (0.22)	0.79 (0.21)*	3.29 (0.66)	3.23 (0.68)
Total cholesterol level, mg/dL	102 (2)	103 (3)	181 (10)*	193 (6)*
Leptin level, ng/mL	2.2 (0.5)	2.4 (0.9)	12.9 (2.5)*	16.0 (4.0)*
TNF-α level, pg/mL	37 (5)	13 (4)*	85 (40)	29 (6)§
Adiponectin level, μg/mL	22 (2)	30 (5)	19 (1)	48 (3)‡
Glucagon level, pg/mL	478 (25)	423 (25)	477 (33)	406 (32)
Visceral adipose tissue				
Visceral adipose tissue weight, mg	559 (57)	564 (77)	1388 (131)*	1331 (94)*
Visceral adipose tissue weight/body weight, mg/g	19.7 (1.7)	19.1 (2.4)	42.5 (3.8)*	42.0 (2.3)*
Adipocyte size, μm^2	1697 (156)	1492 (162)	2787 (324)*	2921 (308)*

Abbreviations: HFD, high-fat diet; KO, β_2-microglobulin knockout mice; SD, standard diet; TNF, tumor necrosis factor; WT, wild type (C57BL/6J) mice.

*$P<0.01$ vs WT-SD.

†$P<0.05$ vs WT-SD.

‡$P<0.01$ vs WT-HFD.

§$P<0.05$ vs WT-HFD.

ameliorated by the depletion of NKT cells. Plasma total cholesterol and leptin levels were also significantly increased by HFD but were not altered in KO-HFD. The plasma adiponectin level did not change in WT-HFD compared with WT-SD, but significantly increased in KO-HFD. The plasma glucagon level tended to be lower in KO-SD compared with WT-SD, which did not reach statistical significance (Table). An HFD significantly increased the weight of visceral adipose tissue compared with groups fed with SD. An HFD significantly increased the weight of visceral adipose tissue compared with the weight of groups fed with SD. In parallel to visceral adipose tissue weight, adipocyte size measured by morphometric analysis was significantly increased in WT-HFD than in WT-SD. However, these increases were not altered in KO-HFD.

In parallel to the glucose intolerance, the infiltration of F4/80-positive macrophages by immunohistochemical staining was significantly increased in visceral adipose tissues from WT-HFD than WT-SD, and this increase was significantly ameliorated in KO-HFD (Figure 2A and B). Major histocompatibility complex (MHC) class II, CD11c, and arginase gene expression, measured by using real-time reverse transcriptase– polymerase chain reaction (a quantitative index of macrophage activation, M1 macrophage, and M2 macrophage, respectively), demonstrated that infiltrating macrophages possess a predominantly M1 phenotype in WT-HFD mice and an M2 phenotype in KO-HFD mice (Figure 2C–E). Taken together, these data indicated that M1 macrophage infiltration was enhanced in adipose tissue from WT-HFD and that this increase was significantly ameliorated in KO-HFD accompanied by a phenotypic change into M2 macrophage.

To examine the temporal relationship between infiltrating NKT cells and macrophages within obese adipose tissues, WT mice were fed with SD or HFD for 2, 4, or 6 weeks. Quantification of NKT cells by Vα14/Jα18 gene expression demonstrated that NKT cell infiltration was significantly increased after 6 weeks of HFD feeding, whereas macrophages quantified by F4/80 gene expression were not increased during the same period in visceral adipose tissues (supplemental Figure 1A and B). Similarly, in subcutaneous fat tissues, NKT cell infiltration was significantly increased after 4 weeks of HFD feeding, whereas macrophages were not increased during the same period (supplemental Figure 1C and D). More important, macrophages were significantly increased at 13 weeks of HFD feeding. Combining the data from weeks 2 to 6 (supplemental Figure 1) with those from week 13 (Figure 2B), the infiltration of NKT cells preceded that of macrophages in obese adipose tissues. Therefore, the occurrence of glucose intolerance and macrophage infiltration into adipose tissue from HFD-induced obese mice is mediated by NKT cells.

To examine the role of NKT cells in gluconeogenesis, phosphoenolpyruvate carboxykinase and glucose-6-phosphatase gene expression were measured in the hepatic tissues. Hepatic gluconeogenesis tended to be suppressed in KO-SD compared with WT-SD, which did not reach statistical significance (supplemental Figure 2).

NKT Cell Activation Exacerbated Metabolic Disorders in HFD-Fed Mice

To further characterize the role of NKT cells in the pathogenesis of HFD-induced glucose intolerance and visceral

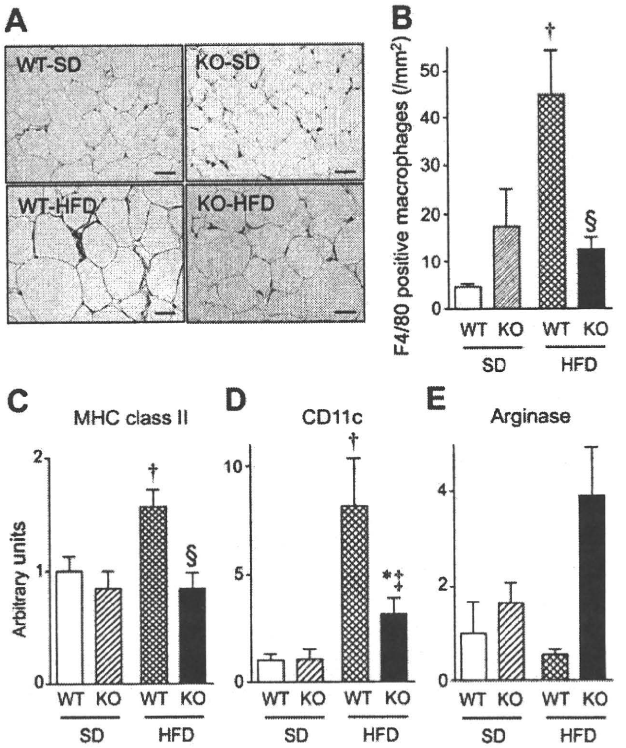

Figure 2. Macrophage infiltration in adipose tissue in experiment 1. A, F4/80 immunohistochemistry. Scale bar, 20 μm. B, The number of F4/80-positive macrophages. C–E, Gene expression of major histocompatibility complex (MHC) class II, CD11c, and arginase, respectively. *$P<0.05$ and †$P<0.01$ vs wild type (WT)–standard diet (SD), and ‡$P<0.05$ and §$P<0.01$ vs WT–high-fat diet (HFD).

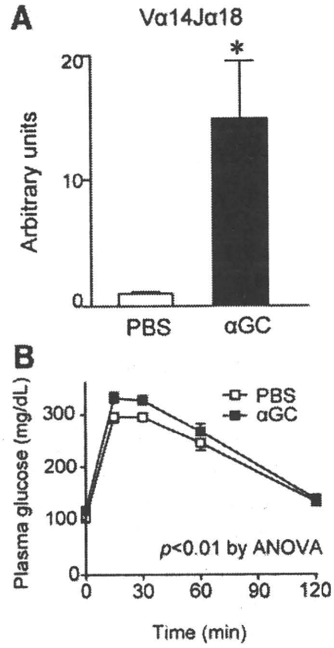

Figure 3. A, Vα14/Jα18 gene expression, an index of natural killer T (NKT) cells, of visceral adipose tissues 8 days after the injection of phosphate-buffered saline (PBS) or α-galactosylceramide (αGC), a specific activator for NKT cells, in experiment 2. B, Plasma glucose concentrations during the intraperitoneal glucose tolerance test (ipGTT) 8 days after PBS or αGC injection. *$P<0.05$ vs PBS.

adipose tissue inflammation, αGC was injected intraperitoneally in WT mice fed HFD for 13 weeks.

αGC did not affect body weight, visceral adipose tissue weight, and adipocyte size in HFD mice 9 days after injection (supplemental Table).

The quantification of NKT cells by Vα14/Jα18 gene expression confirmed αGC significantly enhanced NKT cell infiltration into adipose tissue (Figure 3A). Plasma glucose levels during ipGTT were significantly increased by αGC (15 minutes: 330 [11] vs 296 [11] mg/dL [$P<.05$]; and 30 minutes: 326 [9] vs 295 [8] mg/dL [$P<.05$]) (Figure 3B).

F4/80-positive macrophage infiltration was significantly increased in the adipose tissues for WT mice by αGC (Figure 4A and B). These changes of adipose tissue macrophages by the immunohistochemical analysis were also confirmed by MHC class II and CD11c gene expression (Figure 4C and D). In parallel to macrophage infiltration into the visceral adipose tissue, the injection of αGC significantly increased the expression of MCP-1, TNF-α, IFN-γ, and RANTES genes in HFD mice (Figure 5A–D).

To examine the temporal relationship between infiltrating NKT cells and macrophages, WT mice, aged 8 weeks, were injected using PBS or αGC intraperitoneally and adipose tissues were dissected 1, 4, and 7 days after the injection. The NKT cells and macrophages tended to increase at 4 and 7 days after αGC administration in WT mice (supplemental Figure 3).

To examine the effects of αGC treatment on the metabolic phenotypes of genetically induced obese mice, αGC was injected intraperitoneally in ob/ob mice. Natural killer T cell and macrophage infiltration were significantly increased in αGC-treated ob/ob mice compared with PBS-treated ob/ob mice (supplemental Figure 4A and B). Major histocompatibility complex class II, CD11c, and arginase gene expression were also significantly increased in αGC-treated ob/ob mice (supplemental Figure 4C–E). Similar to diet-induced obese mice, the injection of αGC significantly enhanced the expression of TNF-α, IFN-γ, and RANTES genes, also in ob/ob mice (supplemental Figure 4G–I). Plasma glucose levels during ipGTT in αGC-treated ob/ob mice were comparable to those in PBS-treated ob/ob mice (supplemental Figure 5).

To confirm the specificity of αGC treatment for activating NKT cells, αGC was injected in KO mice fed HFD for 13 weeks. It did not affect NKT cell and macrophage infiltration in the adipose tissues and plasma glucose levels during ipGTT in KO mice (supplemental Figure 6).

To assess the direct relationship between NKT cell activation and adipose tissue inflammation, splenic $CD11b^{+}Gr1^{-}CD4^{-}CD8^{-}B220^{-}$ cells (macrophage-enriched cells) and liver $MHC\text{-}classII^{-}CD8^{-}B220^{-}$ lymphocytes (NKT-enriched cells) were cocultured with or without αGC for 48 hours. Macrophages conditioned with activated NKT cells by αGC secreted a significantly larger amount of MCP-1 into the coculture media compared with unconditioned macrophages (supplemental Figure 7).

Discussion

The present study demonstrated that NKT cells were infiltrated into the visceral adipose tissue in association with

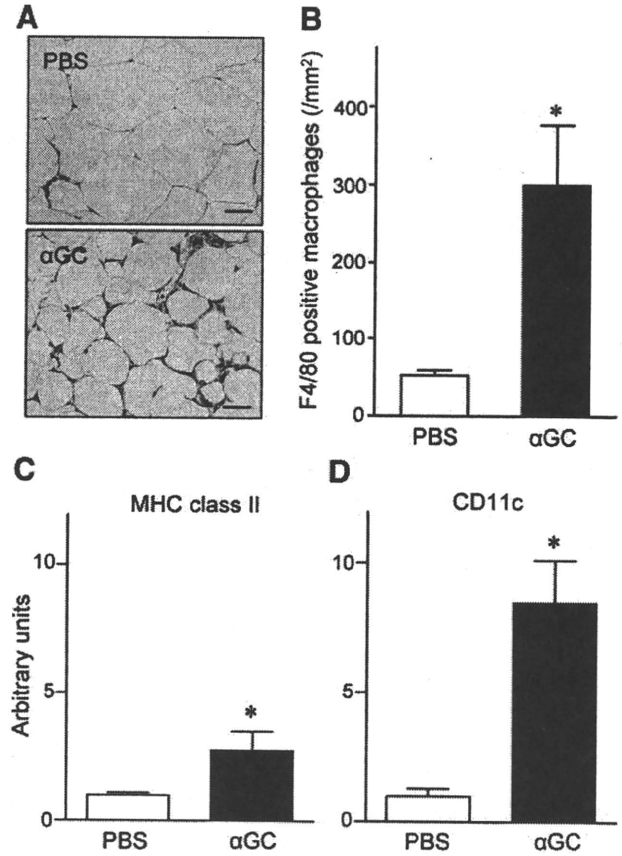

Figure 4. Macrophage infiltration in adipose tissue in experiment 2. A, Demonstrable figures of F4/80 immunohistochemistry. Scale bar, 20 μm. B, The number of F4/80-positive nuclei from mice given phosphate-buffered saline (PBS) and α-galactosylceramide (αGC). C and D, Expression of major histocompatiblity complex (MHC) class II and CD11c genes, respectively, in visceral adipose tissues. $^*P<0.05$ vs PBS.

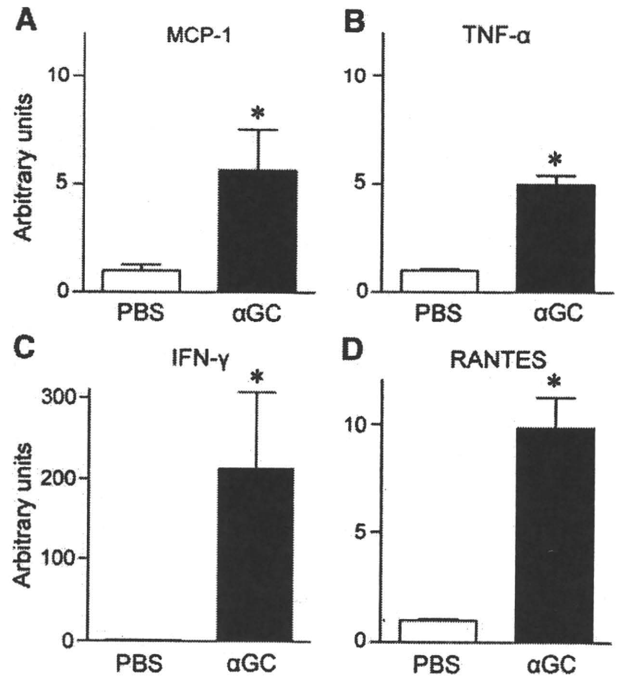

Figure 5. A–D, Expression of monocyte chemoattractant protein (MCP) 1, tumor necrosis factor (TNF) α, interferon (IFN) γ, and regulated upon activation normal T cell expressed secretion (RANTES) genes, respectively, in visceral adipose tissues from mice given phosphate-buffered saline (PBS) and α-galactosylceramide (αGC) in experiment 2. Quantitative reverse transcription (RT)–polymerase chain reaction (PCR) was performed 9 days after PBS or αGC injection. $^*P<0.05$ vs PBS.

macrophages during the development of glucose intolerance in a mouse model of HFD-induced obesity. The depletion of NKT cells in β_2 microglobulin KO mice ameliorated glucose intolerance and visceral adipose tissue inflammation induced by HFD feeding without affecting obesity itself. On the contrary, the activation of NKT cells by αGC exacerbated glucose intolerance and adipose tissue inflammation, including macrophage infiltration and inflammatory cytokine/chemokine gene expression. Therefore, NKT cells may play a pivotal role in the development of glucose intolerance and adipose tissue inflammation associated with HFD-induced obesity.

Visceral obesity has been demonstrated to be associated with macrophage infiltration and inflammation in adipose tissue.[1,2,12] As such, MCP-1 is produced by adipocytes in parallel with increasing adiposity, and mice lacking CCR2, a receptor for MCP-1, exhibit less macrophage infiltration in adipose tissues and a reduction in inflammatory gene expression.[2] However, the development of HFD-induced glucose intolerance was not completely abolished in these mice, suggesting that the other chemokine systems might also contribute to obesity-related adipose tissue inflammation and glucose intolerance.

Early work by cytofluorometric analysis revealed the presence of significant levels of NKT cells in the stromavascular fraction of white adipose tissues.[7] However, the changes of these cells by HFD feeding and even their roles in HFD-induced metabolic disorders have not been examined. In the present study, depleting NKT cells significantly ameliorated glucose intolerance after HFD feeding (Figure 1). Therefore, our study has extended the previous information on the significance of NKT cells by demonstrating that the cell infiltration of these cells into the adipose tissue is involved in the recruitment of macrophages and inflammatory cytokine gene expression during the development of HFD-induced glucose intolerance. However, the present results were not consistent with those of the previous study by Elinav et al,[13] which noted that NKT cells ameliorated glucose intolerance in leptin-deficient ob/ob mice. In their study, the oral administration of liver extracts in ob/ob mice increased hepatic NKT cells and serum levels of IL-10, indicating that the extracts activated NKT cells toward the T_H2 bias, whereas αGC injection stimulated NKT cells toward the T_H1 slant in the present study. Therefore, the discrepancy between these studies might be the result of the differences in the methods of modulating NKT cells and the resultant changes of cytokines subsequent to NKT cell activation. The differences in the animal models (HFD-induced obese mice vs leptin-deficient ob/ob mice) might also be involved in this discrepancy because the injection of αGC significantly enhanced the expression of arginase in ob/ob mice but not in HFD-induced obese mice.

Previous studies demonstrated that proinflammatory T lymphocytes are also present in visceral adipose tissue and contribute to adipose tissue inflammation and the development of glucose intolerance before the recruitment of macrophages.[4] A recent elegant study by Nishimura et al[14] elucidated the role of T lymphocytes in adipose tissue inflammation in obesity. In their study, many $CD8^+$ effector T cells infiltrated into obese epididymal adipose tissue, preceding macrophage infiltration, in HFD-induced obese mice and initiated the inflammatory cascade that leads to insulin resistance in adipocytes. We could not completely exclude the possibility that T lymphocytes are involved in our model because β_2 microglobulin KO mice used in the present study lack not only NKT cells but also $CD8^+$ T lymphocytes.[15] However, the development of both glucose intolerance and adipose tissue inflammation induced by HFD was significantly exacerbated by the specific activation of NKT cells by using αGC, an activator of NKT cells but not T cells (Figures 3–5). Based on these results, we consider that NKT cells are critically involved in glucose intolerance and adipose tissue inflammation in obese mice.

The NKT cells are a specialized lineage of T cells that recognize glycolipid antigens presented by the MHC class I–like molecule CD1d.[16] The NKT cells mediate various functions rapidly by producing a mixture of T_H1 and T_H2 cytokines, such as IFN-γ and IL-4, in shaping subsequent adaptive immune responses.[6] The present study demonstrated that accumulated macrophages in adipose tissues in αGC-treated mice were classically activated (M1) macrophages, one of the distinct subsets of macrophages categorized as M1 by CD11c (Figure 4).[17,18] In agreement with these findings, the activation of NKT cells was associated with increased gene expression of T_H1-cytokine IFN-γ and MCP-1 in HFD-fed mice (Figure 5). Interferon-γ can also promote the recruitment of monocytes by inducing MCP-1 secretion from periadipocytes, and it could activate other cells, such as macrophages. Therefore, cytokines and chemokines, including IFN-γ and MCP-1, were mechanistically involved in the infiltration of macrophages as a result of NKT cell activation. The NKT cells may orchestrate the inflammatory process in adipose tissue in association with the development of glucose intolerance. The beneficial effects of depleting NKT cells are mostly mediated by the reduction of macrophages. It may be informative to examine whether immunosuppressive agents, such as cyclosporine and tacrolimus, which have been shown to suppress αGC-induced cytokine production in murine NKT cells,[19,20] can ameliorate adipose tissue inflammation and glucose intolerance in our model. However, they also induce glucose intolerance via its toxic effects on the pancreatic islet cells.[21,22] Therefore, these reagents may not be suitable for investigating the role of NKT cells in glucose intolerance in HFD-induced obesity in vivo.

The underlying mechanisms responsible for the activation of NKT cells by the HFD feeding remain established. Based on our results using αGC, a glycosphingolipid derived from marine sponges, sphingolipid ceramide may be a crucial intermediate linking between excess nutrients by HFD and inflammatory cytokines to induce glucose intolerance. In fact, ceramide has been shown to be synthesized by long-chain fatty acids and to induce both inflammation and insulin resistance.[23] In agreement with our results, Rocha et al[5] reported that the HFD feeding increases a number of T cells and IFN-γ gene expression in adipose tissue, suggesting T-cell priming toward the T_H1 slant. However, the HFD feeding has been shown to suppress T_H1 responses in B6 mice by inhibiting toll-like receptor–mediated maturation and proinflammatory cytokine production in dendritic cells.[24] The discrepancy between these studies might be the result of the differences in the tissues studied (visceral adipose tissue lymphocytes vs splenic lymphocytes). More important, the contribution of NKT cells is not mediated by the modulation of adipose tissue weight or adipocyte size because these variables did not differ between HFD-fed groups (Table 1 and Supplemental Table); however, adipocyte cell size has been shown to be an independent predictor of glucose intolerance.[25]

Activated macrophages secrete TNF-α, which can inhibit insulin signal transduction.[26] Obesity itself can trigger adipose tissue inflammation, which leads to the desensitization of insulin action.[27] We have demonstrated that NKT cells may be important in the evolution of atherosclerotic lesions by communicating macrophages through cell-cell interactions and/or secreting inflammatory cytokines.[10] Some of the inflammatory processes involved in atherogenesis (as shown in our previous study) resemble adipose tissue inflammation in the present study. Therefore, NKT cells are considered to mediate chronic inflammation in vascular and adipose tissues and can represent a direct and common soil for the development of atherosclerotic cardiovascular disease and diabetes. An in vivo transfer experiment with isolated NKT cells may provide more direct evidence of the cause-and-effect relationship between NKT cells and glucose intolerance associated with HFD-induced obesity. Nevertheless, αGC has been established to be a specific activator for NKT cells and, in fact, it has been used in a variety of disease models to elucidate the pathogenetic role of NKT cells.[28] Therefore, we used αGC administration to activate NKT cells in the present study. There are several limitations to be acknowledged in the present study. First, we only examined the adipose tissue in the present study and did not assess the contribution of liver or skeletal muscle, which can also determine insulin sensitivity.[1] Fasting plasma glucose level and HOMA-IR were significantly lower in KO-SD than in WT-SD (Table). Knockout-SD mice tended to have lower plasma glucose levels and area under the curve values during ipGTT compared with WT-SD (Figure 1B and C); this finding did not reach statistical significance. These data suggested that the absence of NKT cells could improve glucose metabolism in healthy mice, independently of adipose tissue inflammation. It may be possible that NKT cells affect glucose metabolism via the alterations of gluconeogenesis in the liver and skeletal muscle. However, based on the results that the improvement of glucose metabolism is relatively small in KO-SD mice (Figure 1), we consider that NKT cells may impair glucose tolerance predominately via promoting adipose tissue inflammation exclusively in HFD-fed mice. Second, there was massive macrophage infiltration in the adipose tissue in our HFD-fed mice even though the weight gain was relatively small. The NKT cell infiltration preceded macrophage infiltration in obese visceral adipose tissues and may play an important role in the early phase of adipose tissue inflammation. Therefore, even though we have not examined how much NKT cells and macrophages infiltrate within adipose tissues during the development of more severe obesity, we consider that the deletion of NKT cells can effectively attenuate the infiltration of macrophages in this setting. In contrast, the activation of NKT cells has been reported to be protective against type 1 diabetes, systemic lupus erythematosus, and infections.[29] Therefore, the inhibition of NKT cells as a therapeutic strategy to prevent and treat metabolic syndrome and cardiovascular disease for obese individuals needs to be used cautiously in the setting of these disease conditions.

In conclusion, the depletion of NKT cells ameliorated chronic inflammation in visceral adipose tissues and suppressed the development of glucose intolerance in HFD-induced obese mice. On the other hand, the activation of NKT cells exacerbated macrophage infiltration in adipose tissue and glucose intolerance with obesity. Therefore, NKT cells enhance chronic inflammation in visceral adipose tissue and contribute to the development of metabolic disorders in obesity. The NKT cells may be the novel therapeutic targets in atherosclerosis, metabolic syndrome, and type 2 diabetes.

Acknowledgments

We thank Akiko Aita, Miwako Fujii, and Kaoruko Kawai for excellent technical assistance.

Sources of Funding

This study was supported in part by grants 20117004 and 21390236 from the Ministry of Education, Science, and Culture, the Foundation for Total Health Promotion, and the Mitsubishi Pharma Research Foundation.

Disclosures

None.

References

1. Hotamisligil GS. Inflammation and metabolic disorders. *Nature.* 2006; 444:860–867.
2. Weisberg SP, McCann D, Desai M, Rosenbaum M, Leibel RL, Ferrante AW Jr. Obesity is associated with macrophage accumulation in adipose tissue. *J Clin Invest.* 2003;112:1796–1808.
3. Weisberg SP, Hunter D, Huber R, Lemieux J, Slaymaker S, Vaddi K, Charo I, Leibel RL, Ferrante AW. CCR2 modulates inflammatory and metabolic effects of high-fat feeding. *J Clin Invest.* 2006;116:115–124.
4. Wu H, Ghosh S, Perrard XD, Feng L, Garcia GE, Perrard JL, Sweeney JF, Peterson LE, Chan L, Smith CW, Ballantyne CM. T-cell accumulation and regulated on activation, normal T cell expressed and secreted upregulation in adipose tissue in obesity. *Circulation.* 2007;115:1029–1038.
5. Rocha VZ, Folco EJ, Sukhova G, Shimizu K, Gotsman I, Vernon AH, Libby P. Interferon-γ, a Th1 cytokine, regulates fat inflammation: a role for adaptive immunity in obesity. *Circ Res.* 2008;103:467–476.
6. Van Kaer L. NKT cells: T lymphocytes with innate effector functions. *Curr Opin Immunol.* 2007;19:354–364.
7. Caspar-Bauguil S, Cousin B, Galinier A, Segafredo C, Nibbelink M, Andre M, Casteilla L, Penicaud L. Adipose tissues as an ancestral immune organ: site-specific change in obesity. *FEBS Lett.* 2005;579:3487–3492.
8. Ross R. Atherosclerosis–an inflammatory disease. *N Engl J Med.* 1999; 340:115–126.
9. Tupin E, Nicoletti A, Elhage R, Rudling M, Ljunggren HG, Hansson GK, Berne GP. CD1d-dependent activation of NKT cells aggravates atherosclerosis. *J Exp Med.* 2004;199:417–422.
10. Nakai Y, Iwabuchi K, Fujii S, Ishimori N, Dashtsoodol N, Watano K, Mishima T, Iwabuchi C, Tanaka S, Bezbradica JS, Nakayama T, Taniguchi M, Miyake S, Yamamura T, Kitabatake A, Joyce S, Van Kaer L, Onoe K. Natural killer T cells accelerate atherogenesis in mice. *Blood.* 2004;104:2051–2059.
11. Van Kaer L. α-Galactosylceramide therapy for autoimmune diseases: prospects and obstacles. *Nat Rev Immunol.* 2005;5:31–42.
12. Wellen KE, Hotamisligil GS. Obesity-induced inflammatory changes in adipose tissue. *J Clin Invest.* 2003;112:1785–1788.
13. Elinav E, Pappo O, Sklair-Levy M, Margalit M, Shibolet O, Gomori M, Alper R, Thalenfeld B, Engelhardt D, Rabbani E, Ilan Y. Amelioration of non-alcoholic steatohepatitis and glucose intolerance in ob/ob mice by oral immune regulation towards liver-extracted proteins is associated with elevated intrahepatic NKT lymphocytes and serum IL-10 levels. *J Pathol.* 2006;208:74–81.
14. Nishimura S, Manabe I, Nagasaki M, Eto K, Yamashita H, Ohsugi M, Otsu M, Hara K, Ueki K, Sugiura S, Yoshimura K, Kadowaki T, Nagai R. CD8+ effector T cells contribute to macrophage recruitment and adipose tissue inflammation in obesity. *Nat Med.* 2009;15:914–920.
15. Koller BH, Marrack P, Kappler JW, Smithies O. Normal development of mice deficient in β 2M, MHC class I proteins, and CD8+ T cells. *Science.* 1990;248:1227–1230.
16. Godfrey DI, MacDonald HR, Kronenberg M, Smyth MJ, Van Kaer L. NKT cells: what's in a name? *Nat Rev Immunol.* 2004;4:231–237.
17. Lumeng CN, Bodzin JL, Saltiel AR. Obesity induces a phenotypic switch in adipose tissue macrophage polarization. *J Clin Invest.* 2007;117: 175–184.
18. Ricardo SD, van Goor H, Eddy AA. Macrophage diversity in renal injury and repair. *J Clin Invest.* 2008;118:3522–3530.
19. Kajiwara T, Tomita Y, Okano S, Iwai T, Yasunami Y, Yoshikai Y, Nomoto K, Yasui H, Tominaga R. Effects of cyclosporin A on the activation of natural killer T cells induced by α-galactosylceramide. *Transplantation.* 2007;83:184–192.
20. Kato T, Sato Y, Takahashi S, Kawamura H, Hatakeyama K, Abo T. Involvement of natural killer T cells and granulocytes in the inflammation induced by partial hepatectomy. *J Hepatol.* 2004;40:285–290.
21. Ajabnoor MA, El-Naggar MM, Elayat AA, Abdulrafee A. Functional and morphological study of cultured pancreatic islets treated with cyclosporine. *Life Sci.* 2007;80:345–355.
22. Plaumann S, Blume R, Borchers S, Steinfelder HJ, Knepel W, Oetjen E. Activation of the dual-leucine-zipper-bearing kinase and induction of β-cell apoptosis by the immunosuppressive drug cyclosporin A. *Mol Pharmacol.* 2008;73:652–659.
23. Chavez JA, Knotts TA, Wang LP, Li G, Dobrowsky RT, Florant GL, Summers SA. A role for ceramide, but not diacylglycerol, in the antagonism of insulin signal transduction by saturated fatty acids. *J Biol Chem.* 2003;278:10297–10303.
24. Miyazaki Y, Iwabuchi K, Iwata D, Miyazaki A, Kon Y, Niino M, Kikuchi S, Yanagawa Y, Kaer LV, Sasaki H, Onoe K. Effect of high fat diet on NKT cell function and NKT cell-mediated regulation of Th1 responses. *Scand J Immunol.* 2008;67:230–237.
25. Lundgren M, Svensson M, Lindmark S, Renstrom F, Ruge T, Eriksson JW. Fat cell enlargement is an independent marker of insulin resistance and "hyperleptinaemia." *Diabetologia.* 2007;50:625–633.
26. Uysal KT, Wiesbrock SM, Marino MW, Hotamisligil GS. Protection from obesity-induced insulin resistance in mice lacking TNF-α function. *Nature.* 1997;389:610–614.
27. Wellen KE, Hotamisligil GS. Inflammation, stress, and diabetes. *J Clin Invest.* 2005;115:1111–1119.
28. Yu KO, Porcelli SA. The diverse functions of CD1d-restricted NKT cells and their potential for immunotherapy. *Immunol Lett.* 2005;100:42–55.
29. Godfrey DI, Hammond KJ, Poulton LD, Smyth MJ, Baxter AG. NKT cells: facts, functions and fallacies. *Immunol Today.* 2000;21:573–583.

Correction

In the article "Natural Killer T Cells Are Involved in Adipose Tissues Inflammation and Glucose Intolerance in Diet-Induced Obese Mice" by Ohmura et al, which appeared in the February 2010 issue of the journal (*Arterioscler Thromb Vasc Biol.* 2010;30:193–199; DOI: 10.1161/ATVBAHA.109.198614), the publisher omitted several important corrections from the final, published version:

1. Page 193, Affiliations, lines 1 and 3: The Department of Cardiovascular Medicine, Hokkaido University Graduate School of Medicine and the Division of Immunobiology, Institute for Genetic Medicine, Hokkaido University are located in Sapporo, Japan.
2. Page 193, abstract, line 1 of Methods and Results: "To determine whether NKT cells are involved in the development of glucose intolerance" should have been removed and the section should have started with"Male β_2-microglobulin knockout (KO) mice lacking NKT cells. . ."

The online version of the article has been corrected.

The publisher sincerely regrets the errors.

DOI: 10.1161/ATV.0b013e3181f3dc37

(*Arterioscler Thromb Vasc Biol.* **2010;30:e169.**)

***Arterioscler Thromb Vasc Biol* is available at http://atvb.ahajournals.org**

Figure **Plain coronal (A) and gadolinium-enhanced coronal (B) T1-weighted images**

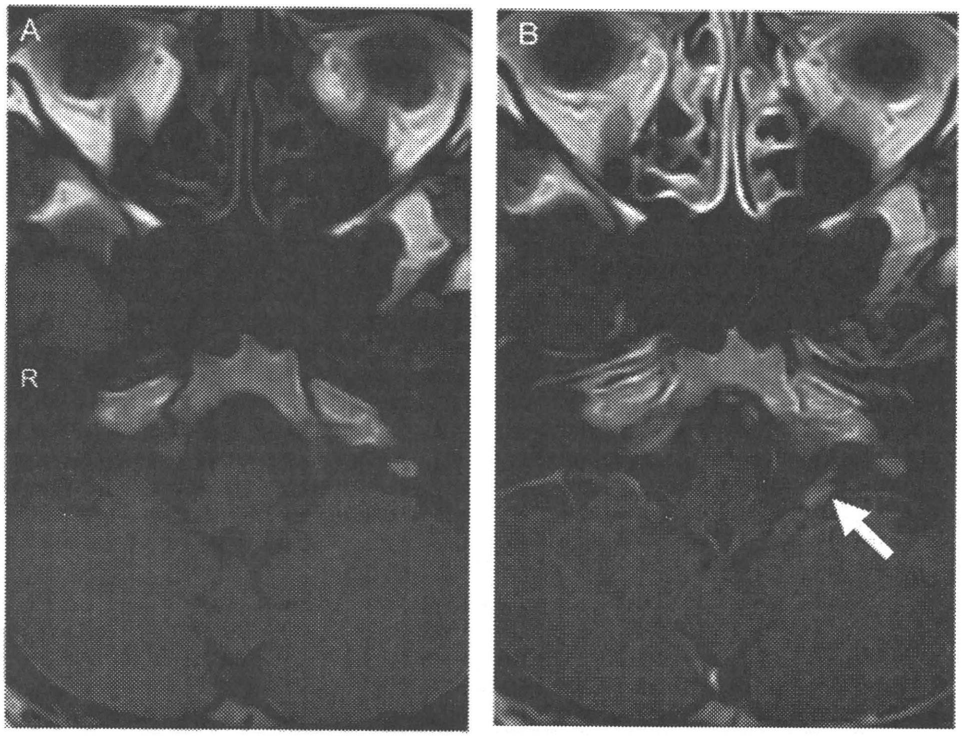

Left glossopharyngeus and vagus nerves are enhanced near the jugular foramen (B arrow).

ministered to ameliorate severe symptoms without sequelae.

From the Department of Neurology, Wakayama Medical University, Wakayama, Japan.

Disclosure: The authors report no disclosures.

Received March 10, 2009. Accepted in final form October 7, 2009.

Address correspondence and reprint requests to Dr. Ken-ya Murata, Department of Neurology, Wakayama Medical University, 840-1 Kimiidera, Wakayama, Japan 641-8510; kemurata@wakayama-med.ac.jp

1. Murakami S, Honda N, Mizobuchi M, Nakashiro Y, Hato N, Gyo K. Rapid diagnosis of varicella zoster virus infection in acute facial palsy. Neurology 1998;51:1202–1205.
2. Osaki Y, Matsubayashi K, Okumiya K, Wada T, Doi Y. Polyneuritis cranialis due to varicella-zoster virus in the absence of rash. Neurology 1995;45:2293.
3. Hayashi T, Murayama S, Sakurai M, Kanazawa I. Jugular foramen syndrome caused by varicella zoster virus infection in a patient with ipsilateral hypoplasia of jugular foramen. J Neurol Sci 2000;172:70–72.
4. Kawabe K, Sekine T, Murata K, et al. A case of Vernet syndrome with varicella zoster virus infection. J Neurol Sci 2008;270:209–210.
5. Gilden DH, Wright RR, Schneck SA, Gwaltney JM, Jr., Mahalingam R. Zoster sine herpete, a clinical variant. Ann Neurol 1994;35:530–533.
6. Mayo DR, Booss J. Varicella zoster-associated neurologic disease without skin lesions. Arch Neurol 1989;46:313–315.

Y. Saitoh, MD
M. Ogawa, MD, PhD
Y. Naito, MD, PhD
Y. Komatsuzaki, MD
H. Tagaya, MD, PhD
K. Arima, MD, PhD
A. Tamaoka, MD, PhD
T. Kitamoto, MD, PhD
M. Murata, MD, PhD

DISCORDANT CLINICOPATHOLOGIC PHENOTYPES IN A JAPANESE KINDRED OF FATAL FAMILIAL INSOMNIA

The GAC→AAC mutation at codon 178 (D178N) of prion protein (PrP) gene (*PRNP*) results in 2 distinct clinicopathologic phenotypes dependent on codon 129 polymorphism of the mutant allele: fatal familial insomnia (FFI) with methionine encoded in codon 129 and familial Creutzfeldt-Jakob disease (CJD) with valine.[1,2] However, some D178N patients who had homozygosity for methionine at codon 129 (D178N-129MM) were reported recently to have the CJD phenotype.[3-5] The cause for these clinicopathologic diversities is unclear. We report a Japanese son–mother pair who presented with FFI and CJD phenotypes.

Case reports. ***Patient 1 (proband).*** A 54-year-old man, born to nonconsanguineous parents, developed dysphagia and loss of appetite. Later, he showed peculiar movement in sleep, followed by insomnia and hypersomnolence. Diplopia, intention tremor, ataxic gait, sleep apnea, fluctuant low-grade fever, tachycardia, hyperhidrosis, constipation, and impotence also

Figure **Histopathologic analysis and Western blot analysis**

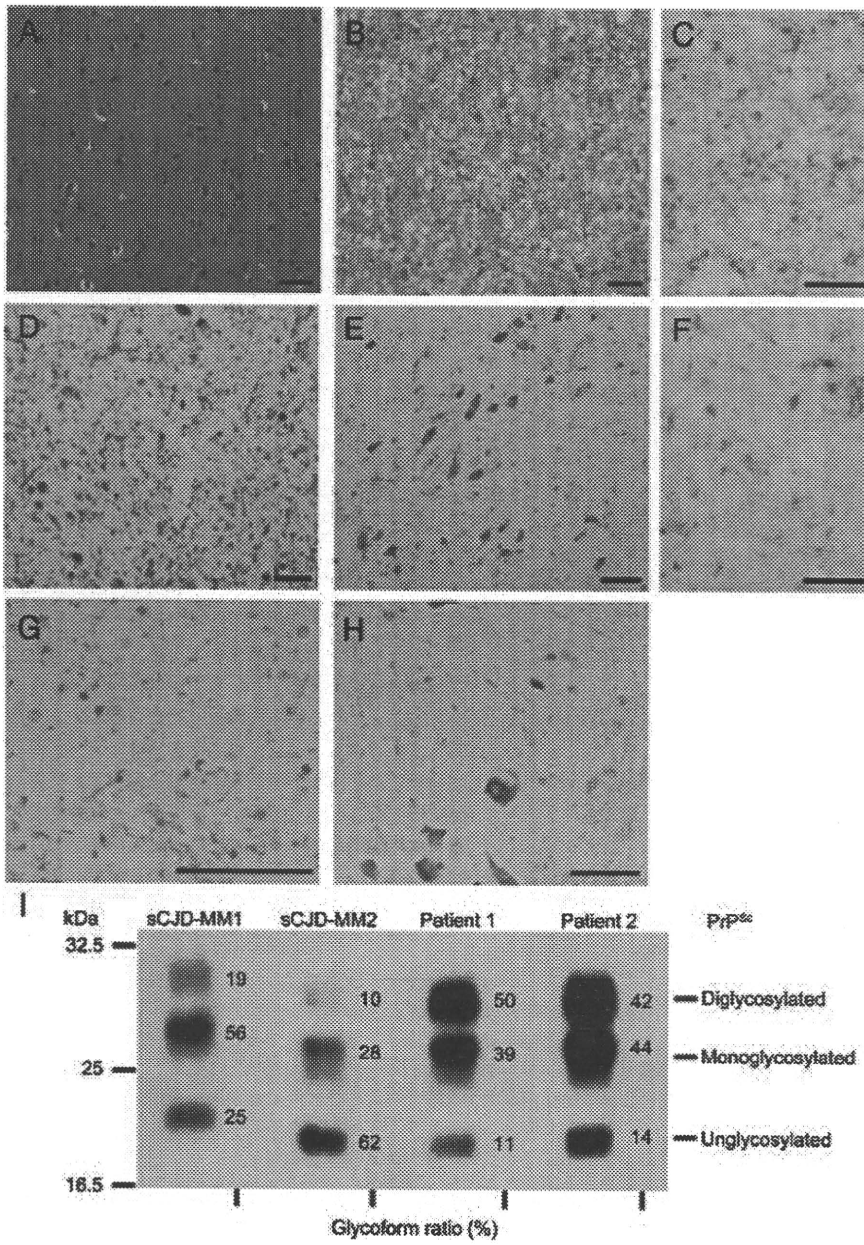

(A–H) Histopathologic findings of patient 1 (A, D, and G) and patient 2 (B, C, E, F, and H); hematoxylin and eosin staining of the frontal cortex (A and B), immunohistochemistry using anti-prion antibody (3F4; Signet Laboratories, Dedham, MA) of the frontal cortex (C) and thalamus (F), Klüver-Barrera staining of the thalamus (D and E) and inferior olivary nucleus (G and H). No spongiform changes were detected in the frontal cortex of patient 1 (or at best partial changes; not shown). In comparison, severe and fine spongiform changes and neuronal loss were detected in patient 2. Patient 1 showed severe neuronal loss and gliosis in the thalamus (D) and inferior olivary nucleus (G). In contrast, patient 2 showed neuronal loss and gliosis, which were mild in the thalamus (E) and moderate in the inferior olivary nucleus (H). Immunohistochemistry in patient 2 showed punctate and coarse granular deposits of pathologic prion protein (PrP^{Sc}) (C) and of the thalamus (F). There also was perivacuolar staining of PrP^{Sc} in places of the cerebral cortex. Coarse granular deposits of PrP^{Sc} in the thalamus were more prominent than that of the cerebral cortex in patient 2. However, immunohistochemistry did not show any PrP^{Sc} deposit throughout the brain in patient 1 (not shown). PrP^{Sc} plaques were not found in either patient. Bar = 50 μm (A, B, D, E, G, and H), 20 μm (C and F). (I) Western blot analysis of patient 1, patient 2, and 2 sporadic Creutzfeldt-Jakob disease (sCJD) patients as disease control was performed with 3F4. Samples of the left two lanes, sCJD-MM1 and sCJD-MM2, were extracted from the sCJD patients who were homozygous for methionine at codon 129 and the types of PrP^{Sc} were type 1 and type 2. The applied amount of frontal cortex tissue was 1.667 mg wet weight in patient 1 and 0.025 mg wet weight in patient 2. Note that both patients 1 and 2 had type 2 PrP^{Sc} as sCJD-MM2. The smallest fragment of PrP^{Sc}, which represents unglycosylated fragment, is weaker than the other 2 fragments in both patients. The PrP^{Sc} glycoform ratio, quantified with Quantity One software using an imaging device, Vasa Doc 5000 (BioRad Laboratories), clarifies that the glycosylation pattern of patient 1 and patient 2 is different from that of sCJD-MM1 and sCJD-MM2. Note the strong band of PrP^{Sc} in patient 2 although a smaller amount of brain tissue was applied than that of patient 1.

followed. He was admitted to hospital 7 months after the onset of symptoms.

Neurologic examination showed mild memory disturbance, cerebellar ataxia, myoclonus, brisk deep tendon reflexes, sleep apnea, and dysautonomia. He did not show akinetic mutism. He moved continuously during sleep. EEG showed no periodic synchronous discharge (PSD), and polysomnography showed loss of deep sleep and marked reduction of REM sleep. Brain MRI showed only mild atrophy. In the cerebral cortex and thalamus, hypoperfusion and hypometabolism were detected by SPECT with ^{99m}Tc-ECD and PET with ^{18}F-2-fluorodeoxy-D-glucose. He died 13 months after the onset of symptoms. *PRNP* analysis, with informed consent, on leukocyte DNA showed D178N-129MM. Histologic examination showed spongiform changes limited to the cingulate gyrus and subiculum, and severe neuronal loss and fibrillary gliosis in the centromedian and dorsomedial nucleus of the thalamus and in the inferior olivary nucleus (figure, A, D, and G). Immunohistochemical analysis showed no pathologic PrP (PrP^{Sc}) deposition in the cerebral cortex, thalamus, or inferior olivary nucleus. Western blot analysis (WB) showed very small amount of type 2 PrP^{Sc} and the same glycosylation pattern of PrP^{Sc} as FFI (figure, I).[6,7]

Patient 2 (mother). A 60-year-old woman showed rapidly progressive dementia. She became mute 5 months later. Neurologic examination showed rigidity and brisk deep tendon reflexes, but no ataxia. EEG showed no PSD. She developed akinetic mutism and died in 1987, 14 months after the onset of symptoms. Histopathologic examination showed spongiform changes throughout the cerebral cortex, and mild neuronal loss and fibrillary gliosis in the dorsomedial nucleus of the thalamus and moderate neuronal loss in the inferior olivary nucleus (figure, B, E, and H). Immunohistochemical analysis of PrP^{Sc} visualized punctate and coarse granular deposits throughout the cerebral cortex (figure, C), and coarse granular deposits in thalamus (figure, F). Although the clinical course and histopathologic findings of patient 2 were compatible with CJD phenotype, the type and glycosylation pattern, including glycoform ratio, of PrP^{Sc} analyzed by WB were the same as patient 1, who presented as typical FFI (figure, I). However, a larger amount of PrP^{Sc} was detected than that of patient 1. *PRNP* analysis on preserved frozen brain tissue, performed with informed consent, revealed exactly the same as patient 1, D178N-129MM.

Discussion. A few reports describe the CJD phenotype in a genetically confirmed D178N-129MM kindred,[3-5] although one kindred showed both FFI and CJD phenotypes within the same family.[5] That kindred and ours indicate that certain factors other than codon 129 polymorphism in the normal allele determine the clinicopathologic phenotype of D178N-129MM.

Our WB suggests the causes of this clinicopathologic diversity. The detection of the larger amount of PrP^{Sc} in patient 2 than in patient 1 may indicate that the amount of PrP^{Sc} is related to the clinicopathologic D178N-129MM phenotype. However, the mechanism by which there is an increased amount of PrP^{Sc} in this kindred is unknown. In addition, that both patients have the same type 2 PrP^{Sc} indicates that the type of PrP^{Sc} may not be related to the D178N-129MM phenotype, unlike sporadic CJD.[6] Finally, the result that the both patients have the same glycosylation pattern of PrP^{Sc}, including glycoform ratio, also indicates that the D178N-129MM phenotype may not be influenced by glycosylation pattern. However, because the glycosylation pattern reflects both the degree of glycosylation and location at which the PrP is cleaved by protease, careful investigation of the glycosylation of PrP is necessary to interpret the clinicopathologic diversity of this D178N-129MM kindred.

The majority of D178N-129 M kindred follows the genetic pattern[1,2]; however, there are a few D178N-129MM kindred who presented with both FFI and CJD phenotypes. Therefore, our kindred may be an exception, suggesting the importance of WB to investigate this rare syndrome.

From the Departments of Neurology (Y.S., M.O., M.M.), Laboratory Medicine (H.T., K.A.), and Psychiatry (K.A.), National Center Hospital of Neurology and Psychiatry, Tokyo; Department of Degenerative Neurological Diseases (Y.S.), National Institute of Neuroscience, National Center of Neurology and Psychiatry, Tokyo; Hatsuishi Hospital (Y.N., Y.K.), Chiba; Department of Neurology (Y.N.), Mie University Graduate School of Medicine, Mie; Miraidaira Clinic (Y.K.), Ibaraki; Mental Health Department of Health Science (H.T.), School of Allied Health Sciences, Kitasato University, Kanagawa; Department of Neurology (A.T.), Doctoral Program in Medical Sciences for Control of Pathological Processes, Graduate School of Comprehensive Human Sciences, University of Tsukuba, Ibaraki; and Division of CJD Science and Technology (T.K.), Department of Prion Research, Tohoku University Graduate School of Medicine, Miyagi, Japan.

Study funding: Supported by a grant from the Research Committee on Prion Diseases and Slow Virus Infection and Research Grant 19A-4 for Nervous and Mental Disorders, Ministry of Health, Labour, and Welfare, Japan.

Disclosure: Dr. Saitoh and Dr. Ogawa report no disclosures. Dr. Naito has received research support from Asubio Pharmaceuticals, Inc., Janssen, Otsuka Pharmaceutical Co. Ltd., and Ono Pharmaceutical Co. Ltd. Dr. Komatsuzaki reports no disclosures. Dr. Tagaya received funding for travel from Sanofi-Aventis, serves on speakers' bureaus for Sanofi-Aventis, Astellas Pharma Inc., Takeda Pharmaceutical Company Limited, Boehringer Ingelheim, and KYORIN Pharmaceutical Co., Ltd., and receives research support from the Ministry of Health, Labour, and Welfare, Japan, Ministry of Education, Culture, Science and Technology, Japan, and Kitasato University School of Allied Health Sciences. Dr. Arima reports no disclosures. Dr. Tamaoka serves on a scientific advisory board for

Chugai Pharmaceutical Company and has received research support from Sankyo Seimei, Ministry of Health, Labour, and Welfare, Japan, and Ministry of Education, Culture, Science and Technology, Japan. Dr. Kitamoto reports no disclosures. Dr. Murata serves on speakers' bureaus for Dainippon Sumitomo Pharma Co., Ltd., Novartis, Boehringer Ingelheim, and GlaxoSmithKline and receives research support from the Ministry of Health, Labour, and Welfare, Japan.

Received February 1, 2009. Accepted in final form October 13, 2009.

Address correspondence and reprint requests to Dr. Miho Murata, Department of Neurology, National Center Hospital of Neurology and Psychiatry, 4-1-1 Ogawahigashimachi, Kodaira, Tokyo 187-8551, Japan; mihom@ncnp.go.jp

ACKNOWLEDGMENT

The authors thank Dr. Hidehiro Mizusawa, Department of Neurology and Neurological Science, Graduate School, Tokyo Medical and Dental University; Dr. Akihide Mochizuki, Department of Neurology, Doctoral Program in Medical Sciences for Control of Pathologic Processes, Graduate School of Comprehensive Human Sciences, University of Tsukuba; and Dr. Yuko Saito, Department of Laboratory Medicine, National Center Hospital of Neurology and Psychiatry, for their comments on the histopathologic data.

1. Medori R, Tritschler HJ, LeBlanc A, et al. Fatal familial insomnia, a prion disease with a mutation at codon 178 of the prion protein gene. N Engl J Med 1992;326:444–449.
2. Goldfarb LG, Petersen RB, Tabaton M, et al. Fatal familial insomnia and familial Creutzfeldt-Jakob disease: disease phenotype determined by a DNA polymorphism. Science 1992;258:806–808.
3. McLean CA, Storey E, Gardner RJ, Tannenberg AE, Cervenakova L, Brown P. The D178N (cis-129M) "fatal familial insomnia" mutation associated with diverse clinicopathologic phenotypes in an Australian kindred. Neurology 1997;49:552–558.
4. Harder A, Jendroska K, Kreuz F, et al. Novel twelve-generation kindred of fatal familial insomnia from Germany representing the entire spectrum of disease expression. Am J Med Genet 1999;87:311–316.
5. Zarranz JJ, Digon A, Atares B, et al. Phenotypic variability in familial prion diseases due to the D178N mutation. J Neurol Neurosurg Psychiatry 2005;76:1491–1496.
6. Parchi P, Giese A, Capellari S, et al. Classification of sporadic Creutzfeldt-Jakob disease based on molecular and phenotypic analysis of 300 subjects. Ann Neurol 1999;46:224–233.
7. Monari L, Chen SG, Brown P, et al. Fatal familial insomnia and familial Creutzfeldt-Jakob disease: different prion proteins determined by a DNA polymorphism. Proc Natl Acad Sci USA 1994;91:2839–2842.

EJN EUROPEAN JOURNAL OF NEUROSCIENCE

European Journal of Neuroscience, Vol. 31, pp. 1155–1163, 2010 doi:10.1111/j.1460-9568.2010.07152.x

MOLECULAR AND DEVELOPMENTAL NEUROSCIENCE

In vitro differentiation of lineage-negative bone marrow cells into microglia-like cells

Daisuke Noto,[1] Kazuya Takahashi,[1,2] Sachiko Miyake[3] and Masahito Yamada[1]
[1]Department of Neurology and Neurobiology of Aging, Kanazawa University Graduate School of Medical Science, Kanazawa, Japan
[2]Department of Neurology, National Hospital Organization Iou National Hospital, Kanazawa, Japan
[3]Department of Immunology, National Institute of Neuroscience, National Center of Neurology and Psychiatry, Tokyo, Japan

Keywords: astrocyte, GFP mice, primary mixed glial culture, TREM2

Abstract

Microglia are believed to be the only resident immune cells in the CNS, originating from hematopoietic-derived myeloid cells and invading the CNS during development. However, the detailed mechanisms of differentiation and transformation of microglial cells are not fully understood. Here, we demonstrate that murine microglial cells show two morphological forms *in vitro*, namely, small round cells expressing CD11b, Iba1, triggering receptor expressing on myeloid cells-2 (TREM2), and weakly expressing major histocompatibility complex class II and large flat cells expressing only CD11b and Iba1. Moreover, lineage-negative bone marrow (LN) cells cultured with primary mixed glial culture cells could differentiate into only the small round microglia-like cells, despite the absence of CCR2 and Gr-1 expression. Addition of macrophage colony stimulating factor (M-CSF) to LN cell culture allowed the proliferation and expression of TREM2 in LN cells, and the addition of neutralizing anti-M-CSF antibodies suppressed the proliferation of LN cells despite the expression of TREM2. When LN cells were cultured with M-CSF, the number of small round cells in the culture was considerably low, indicating that the small round morphology of the immature cells is not maintained in the presence of only M-CSF. On the other hand, when LN cells were grown in the presence of astrocytes, the small round cells were maintained at a concentration of approximately 30% of the total population. Therefore, cell–cell contact with glial cells, especially astrocytes, may be necessary to maintain the small round shape of the immature cells expressing TREM2.

Introduction

Microglia are believed to be the only resident immune cells in the CNS; they develop from hematopoietic-derived myeloid cells and invade the CNS during development (Ling & Wong, 1993). Microglial cells are recognized to play an important role not only in neuroinflammatory and neurodegenerative diseases, such as multiple sclerosis and Alzheimer's disease, but also in neuroprotective and anti-neuroinflammatory processes (Akiyama & McGeer, 2004; Sanders & De Keyser, 2007; Takahashi *et al.*, 2007). In a recent study, it has been reported that physiological microglial phagocytosis induced the efficient removal of apoptotic cells and cellular debris without inflammatory processes; this process is expected to be a novel, attractive target for protection from neuroinflammation or neurodegeneration (Takahashi *et al.*, 2005, 2007; Neumann & Takahashi, 2007). The detailed mechanisms underlying the differentiation and transformation of microglial cells, however, are not fully understood. Even in adulthood, hematopoietic-derived cells develop into resident perivascular macrophages and microglia (Hickey & Kimura, 1988; Priller *et al.*, 2001; Simard & Rivest, 2004). Although the exact cellular subtype of myeloid precursors that develop into microglia is unknown, it has been reported that only Ly-6C^{high} CCR2+ monocytes can invade and differentiate into perivascular microglia (Mildner *et al.*, 2007).

The bone marrow produces new blood cells, including all cell types of the myeloid lineage, some of which may differentiate into microglia. Lineage-negative bone marrow (LN) cells are defined by the absence of surface markers, such as CD3, CD4, CD5, CD8α, CD11b/MAC-1α, B220, Gr-1 and TER-119, and are considered to comprise many hematopoietic precursors, including microglia precursors. Thus, LN cells might represent microglial precursors and may serve as a natural vehicle for CNS cells in gene therapy.

In this study, we show that murine microglial cells are present *in vitro* in two morphological forms, namely, as small round cells expressing CD11b, Iba1, triggering receptor expressing on myeloid cells-2 (TREM2), and weakly expressing major histocompatibility complex (MHC) class II and as large flat cells expressing only CD11b and Iba1. We found that LN cells could differentiate into the small round-type but not the large flat-type microglia-like cells. Moreover, we concluded that not only macrophage colony-stimulating factor (M-CSF) but also cell–cell contacts with astrocytes play an important role in microglial differentiation.

Correspondence: Dr K. Takahashi, [2]Department of Neurology, as above.
E-mail: ktakaha@ioudom.hosp.go.jp

Received 26 May 2009, revised 8 January 2010, accepted 27 January 2010

Materials and methods

Isolation of LN cells from adult green fluorescence protein (GFP) mice bone marrow

Bone marrow cells were collected from 8- to 10-week-old C57BL/6 mice (Charles River, Japan) or GFP transgenic mice on a C57BL/6 mice background that were kindly provided by Dr Masaru Okabe (Osaka University, Japan) by flushing out the femora and tibiae of the hind limb under deep anesthesia by the diethyl ether. Erythrocyte removal was performed by lysis with the Mouse Erythrocyte Lysing Kit (R&D, Minneapolis, MN, USA). For eliminating lineage marker-positive cells via negative selection, bone marrow cells were incubated at 4°C for 30 min with eight types of rat monoclonal antibodies against mice lineage markers [CD3, CD4, CD5, CD8α, CD11b/MAC-1α, B220, Gr-1 and TER-119 (R&D)]. The cells were then washed and incubated with immunomagnetic beads (Invitrogen, Tokyo, Japan) at 4°C for 30 min. Finally, LN cells were collected by the removal of lineage marker-positive bone marrow cells by using a magnet stand that attracted the lineage marker-positive cells attached to the antibodies.

All experiments were approved by the Ethics Committee of Kanazawa University, and performed in accordance with the guidelines of the local animal care and use committee of Kanazawa University.

Primary mixed glial cell culture

Microglial cells were prepared from the brains of postnatal days 3–5 (P3–P5) C57BL/6 mice under deep anesthesia by the diethyl ether, as previously described (Takahashi *et al.*, 2005). Briefly, meninges were removed mechanically, and the cells were dissociated by trituration and cultured in basal medium Eagle (Invitrogen), 10% fetal calf serum (Invitrogen), 1% glucose (Sigma, Tokyo, Japan), 1% L-glutamine (Invitrogen) and 1% penicillin/streptomycin (Invitrogen) for 14 days to form a confluent glial monolayer. LN cells obtained from GFP mice were added onto the confluent glial monolayer.

Treatment of LN cell culture with mixed glial cell culture supernatant, neutralizing antibodies or cytokines

LN cells were cultured with the mixed glial cell culture supernatant obtained from the Day 14 primary mixed glial culture. LN cells were also cultured with a culture medium containing M-CSF (10 ng/mL; Peprotech, Rocky Hill, NJ, USA), tumor necrosis factor-α (TNF-α; 10 ng/mL; Peprotech) or vascular endothelial growth factor (VEGF; 50 ng/mL; Peprotech) for 7 days. For the neutralizing assay, anti-M-CSF (2 μg/mL; R&D), anti-TNF-α (2 μg/mL; R&D) or anti-VEGF (1 μg/mL; R&D) antibodies were added in the LN cell culture for 7 days.

Immunohistochemistry

Mixed glial cell cultures with or without GFP-positive (GFP+) LN cells were fixed in 4% paraformaldehyde for 1 h, blocked by Protein Block (Dako, Denmark) for 2 h, and then immunostained with monoclonal rat antibodies directed against CD11b (Serotec, Oxford, UK) and a secondary fluorescence rhodamine-conjugated antibody directed against rat IgG (1 : 200; Millipore, Billerica, MA, USA). To identify the cell type, cells were double-labeled with a purified polyclonal sheep antibody directed against TREM2 (1 : 50, R&D), monoclonal rabbit antibodies directed against Iba1 (Wako, Kanagawa, Japan), and glial fibrillary acidic protein (GFAP; Dako) and monoclonal mouse antibodies directed against IAb (BD Pharmingen, Tokyo, Japan), followed by a secondary fluorescein isothiocyanate (FITC)-conjugated antibody directed against mouse IgG. Images were collected by fluorescence microscopy with a 20 × objective (Olympus, Tokyo, Japan). A confocal microscope with a 40 × objective (Zeiss, Jena, Germany) was used to obtain Z-stack images, and series of optical sections (512 × 512 pixels, pixel size: 440 nm) were collected at intervals of 380 nm. Images were analysed using the Zeiss LSM Image browser (Zeiss).

To quantify the number of cells, 10 fields under the 20 × objective were randomly selected and photographed by fluorescence microscopy using a digital camera (Olympus) for each experiment. Total cells, GFP-positive cells and positively immunostained cells were classified and counted according to their morphology.

Isolation of microglia and splenic macrophages

Microglial cells and GFP+ LN cells-derived microglial cells in primary mixed glial culture were obtained by shaking the flasks at 0.25 *g* for 2 h. Adult CNS microglia and splenic macrophages were obtained from GFP mice. The cortex and spinal cord of GFP mice were isolated and homogenized. Homogenates were incubated with 0.3 Wunsch units/mL Liberase Blendzyme 3 (Roche, Tokyo, Japan) and 0.1 mg/mL DNaseI (Roche) in RPMI 1640 medium at 37°C for 30 min. Microglia were separated through a density gradient. The cells were suspended in 27% Percoll (GE Healthcare, Tokyo, Japan) and overlaid with a 72% gradient. The density gradient was centrifuged at 1500 *g* for 30 min at 4°C. Myelin collected in the 27% Percoll layer was removed. The majority of microglia were found in the interface of the 27 and 72% Percoll layers. Cells were obtained from this interface and washed from the Percoll with phosphate-buffered saline. The spleen was isolated and cut into small fragments. Cells were incubated with 0.3 Wunsch units/mL Liberase Blendzyme 3 (Roche) and 0.1 mg/mL DNaseI (Roche) in RPMI 1640 medium at 37°C for 45 min. Erythrocyte removal was performed using ACK solution.

Flow cytometry analysis of LN cells, microglia and splenic macrophages

For flow cytometry analysis, cells were first incubated for Fc-receptor blockade by CD16/CD32 antibody (BD Pharmingen) and then stained with phycoerythrin (PE)-conjugated anti-IAb antibody and anti-CD45 antibody (BD Pharmingen), PerCP-Cy5.5-conjugated anti-CD11b antibody (BD Pharmingen), APC-conjugated anti-TREM2 antibody (R&D) and anti-F4/80 antibody (eBioscience, San Diego, CA, USA), or purified anti-CCR2 antibody (Abcam, Tokyo, Japan) followed by rhodamine-conjugated anti-Goat IgG (Millipore). Analysis was performed with a FACSCalibur flow cytometer (BD Biosciences, Tokyo, Japan).

Proliferation assay

Microglial cells and GFP+ LN cells-derived microglia-like cells in primary mixed glial culture, adult CNS microglia and splenic macrophages were cultured with various concentrations of M-CSF (0–100 ng/mL), and cultures were pulsed with 1 mCi of [^{3}H]TdR (MP Biomedicals, Tokyo, Japan) for the last 16 h of the incubation. Cell incorporation of [^{3}H]TdR was counted with a Topcount (Perkin Elmer, Boston, MA, USA). The mean cpm of triplicate cultures was calculated.

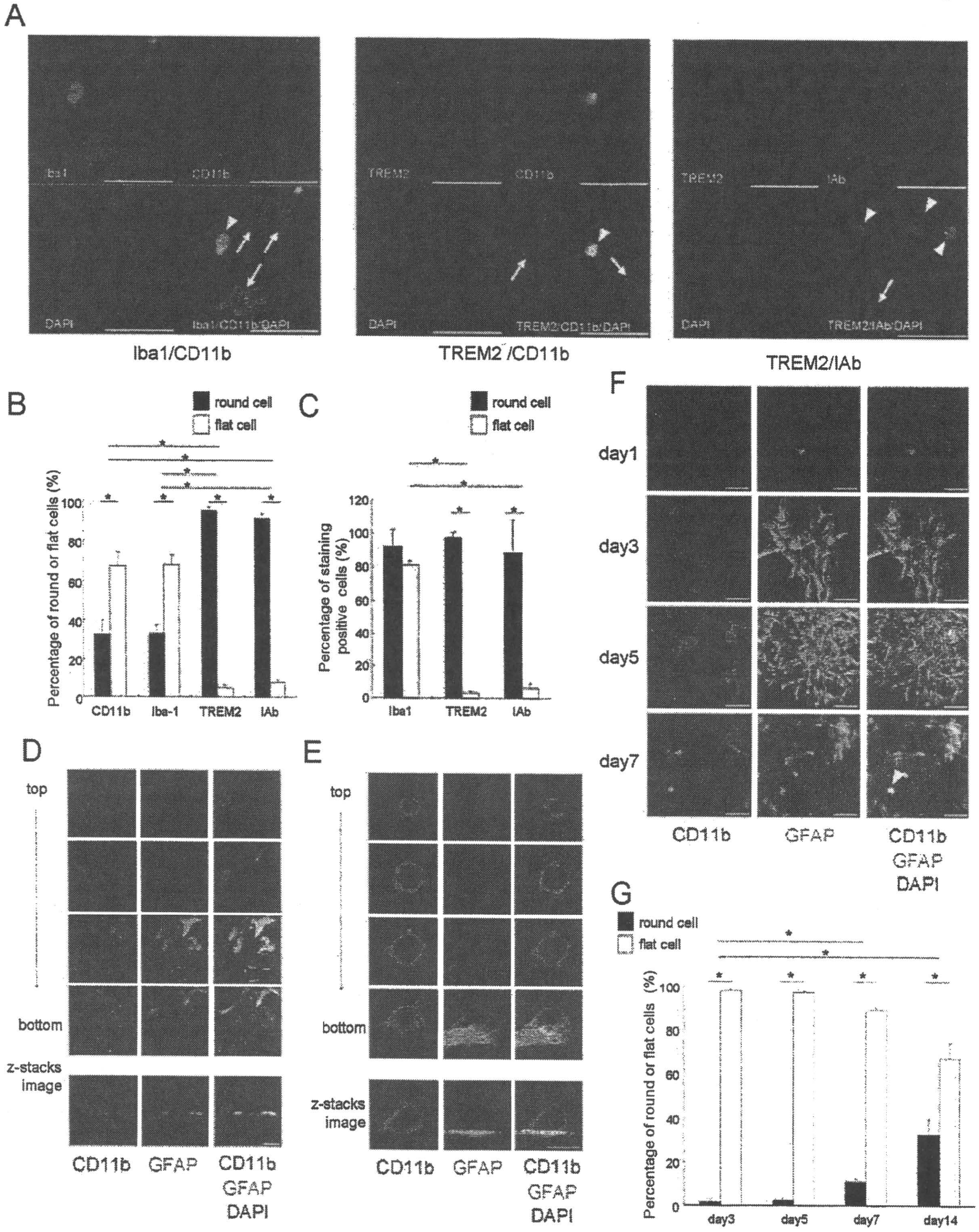

FIG. 1. Morphology of microglia in primary mixed glial culture. (A) Immunocytology of primary mixed glial culture stained with anti-Iba1, anti-triggering receptor expressing on myeloid cells-2 (TREM2) anti-IAb, anti-CD11b and 4′,6-diamidino-2-phenylindole (DAPI). Arrowheads indicate small round cells. Arrows indicate large flat cells. Scale bar: 50 μm. (B) The percentage of round cells or flat cells among staining-positive cells was quantified by microscopic analysis. Data are presented as mean ± standard deviation (SD). (C) The percentage of Iba-1-, TREM2- or IAb-positive cells among CD11b-positive (CD11b+) round or flat cells was quantified by microscopic analysis. Data are presented as mean ± SD. (D) *Z*-stack immunofluorescence confocal microscopy of primary mixed glial culture stained with anti-CD11b (red), anti-glial fibrillary acidic protein (GFAP; green) and DAPI (blue). Scale bar: 10 μm. (E) *Z*-stack immunofluorescence confocal microscopy of primary mixed glial culture stained with anti-CD11b (red), anti-GFAP (green) and DAPI (blue). Scale bar: 10 μm. (F) Immunocytology of primary mixed glial culture. Cultures were fixed at Days 1, 3, 5 and 7 of the culture and stained with primary anti-CD11b and anti-GFAP antibodies followed by rhodamine- or FITC-conjugated secondary antibody and DAPI. Arrowheads indicate small round cells. Scale bar: 50 μm. (G) The percentage of CD11b+ round or flat cells was quantified by microscopic analysis. Data are presented as mean ± SD; $^*P \leq 0.05$. Data are representative of three independent experiments.

Stimulation by anti-TREM2 antibody

Small round cells were added to culture dishes coated with the anti-TREM2 monoclonal antibody (R&D) or control antibody, and centrifuged at 400 *g* for 5 min. After 60 min, the cells were fixed at a final concentration of 4% formaldehyde for 10 min at 37°C. Following centrifugation, the supernatant was removed, and the cells were resuspended in 90% ice-cold methanol and incubated for 30 min at 4°C. Cells were washed and stained with Alexa 647-conjugated anti-phospho-ERK1/2 antibody (Cell Signaling Technology, Tokyo, Japan) for 30 min. Analysis was performed using a FACSCalibur flow cytometer.

Bio-Plex cytokine assay system

Culture supernatant samples were analysed simultaneously for 17 different cytokines and chemokines (IL-1b, IL-2, IL-4, IL-5, IL-10, GM-CSF, IFN-γ, TNF-α, IL-15, IL-18, FGF-basic, LIF, M-CSF, MIG, MIP-2, PDGF-BB and VEGF) using the Bio-Plex Cytokine Assay System (Bio-Rad Laboratories, Hercules, CA, USA), according to the manufacturer's instructions. Briefly, 50 μL of each sample and standard (Bio-Rad) was added to 50 μL of antibody-conjugated beads (Bio-Rad) in a 96-well filter plate (Millipore). After 30-min incubation, the plate was washed, and 25 μL of a biotinylated antibody solution (Bio-Rad) was added to each well, followed by 30-min incubation again. The plate was washed, and 50 μL of streptavidin-conjugated PE (Bio-Rad) was added to each well and incubated for 10 min. After a final wash, the contents of each well were resuspended in 125 μL of assay buffer (Bio-Rad) and analysed using a Bio-Plex Array Reader (Bio-Rad). The lower detection limit for each cytokine or chemokine was 2 pg/mL.

Statistical analysis

Data are presented as mean ± SD of at least three independent experiments. Data were analysed by the Mann–Whitney *U*-test to determine significant differences.

Results

Characterization of microglia in the primary mixed glial culture

To characterize microglial cells in the mixed glial culture, we stained several microglia markers such as Iba1, CD11b, TREM2 and IAb (MHC class II molecule of C57/BL6 mice) on the cultured microglial cells (Fig. 1A). CD11b-positive (CD11b+) cells in the primary mixed glial culture showed two major morphological forms, namely, small round-shaped cells (32.8 ± 6.9% SD of CD11b+ cells) expressing Iba1, TREM2 and IAb (Iba1+ cells, 91.9 ± 10.2% SD; TREM2+ cells, 97.5 ± 3.5% SD; IAb+ cells; 88.9 ± 19.2% SD), and large flat cells (67.2 ± 6.9% SD of CD11b+ cells) expressing only Iba1 (Iba1+ cells, 81.1 ± 2.6% SD; TREM2+ cells, 3.3 ± 1.1% SD; IAb+ cells, 6.4 ± 2.8% SD; Iba1 vs. TREM2, $P = 0.0495$; Iba1 vs. IAb, $P = 0.0495$; Fig. 1B and C). *Z*-sectioned scans by confocal microscopy revealed that small, spherically shaped cells lay above the astrocytes, and large flat cells lay under the astrocytes (Fig. 1D). Moreover, the spherical cells appeared to have extended processes toward the astrocytes (Fig. 1E).

To investigate the time point at which both the forms of the microglial cells appeared in the primary mixed glial culture, we performed a kinetic study. At Day 1 after the culture of mixed glial cells, CD11b+ cells showed a small amoeboid shape (Fig. 1F). At Day 3, the CD11b+ cells assumed a larger flat shape. Small round CD11b+ cells were very few in number until Day 5 (Day 3, 1.9 ± 1.1% SD; Day 5, 2.7 ± 0.9% SD), but increased greatly after Day 7 (Day 7, 10.9 ± 1.1% SD vs. Day 3, $P = 0.0495$; Day 14, 32.8 ± 6.9% SD vs. Day 3, $P = 0.0495$; Fig. 1F and G).

Characteristics of LN cells

LN cells were isolated by negative selection using magnet beads. The purity of LN cells after negative selection by flow cytometry was consistently above 90% on several examinations (Fig. 2A). LN cells expressed neither the microglia marker TREM2 nor CD11b, which is one of the lineage markers for negative selection (Fig. 2B). No expression of CCR2 or Gr-1 (lineage markers for negative selection) was detected on the LN cells, which have previously been described as

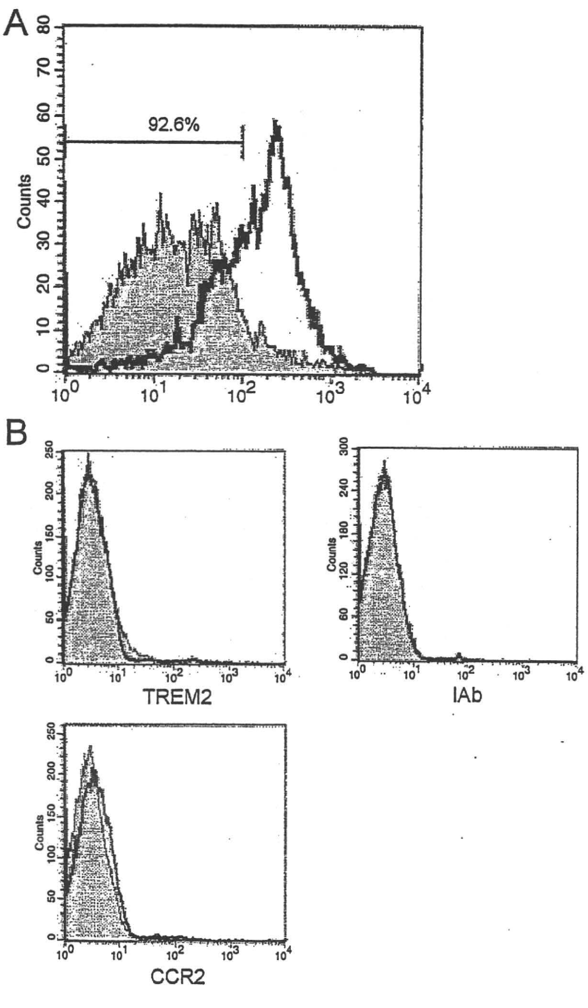

FIG. 2. Flow cytometry analysis of LN cells. (A) Flow cytometry analysis of LN cells (filled histogram) and bone marrow cells (open histogram) stained with rat monoclonal antibodies against mice lineage markers (CD3, CD4, CD5, CD8α, CD11b/MAC-1α, B220, Gr-1 and TER-119). Numbers above the lines indicate the percentage of LN cells. (B) Flow cytometry analysis of LN cells. Filled histograms, staining with antibodies to markers below plots; open histograms, isotype-matched control antibody. Data are representative of three independent experiments. TREM2, triggering receptor expressing on myeloid cells-2.

markers of microglial precursors (Fig. 2B). IAb, which is an MHC class II antigen, was negative on the surface of the LN cells.

Differentiation of LN cells into microglia-like cells

LN cells obtained from GFP mice were co-cultured with primary mixed glial cells for 2 weeks. Two weeks after the co-culture, the cells were stained by anti-TREM2, anti-Iba1, anti-MHC class II and anti-CD11b antibodies, followed by rhodamine- or Cy3-conjugated secondary antibodies (Fig. 3A). GFP+ cells showed two major morphologies, i.e. small and round cells with bright nuclei (27.7 ± 7.9% SD in GFP+ cells) and flat cells with dark nuclei (69.9 ± 6.9% SD in GFP+ cells), similar to the microglia in the primary mixed glial cells seen in Fig. 1. Most of the small round cells were TREM2-, Iba1-, CD11b- and IAb-positive (TREM2+ cells, 92.7 ± 1.9% SD; Iba1+ cells, 93.6 ± 1.6% SD; CD11b+ cells, 96.5 ± 3.1% SD; IAb+ cells, 84.6 ± 13.4% SD; Fig. 3B), and were spherically shaped along the *z*-axis (Fig. 3C). On the other hand, flat cells expressed none of the following: CD11b, Iba1, TREM2 or IAb (TREM2+ cells, 6.5 ± 3.9% SD; Iba1+ cells, 3.5 ± 1.0% SD; CD11b+ cells, 9.3 ± 3.7% SD; IAb+ cells, 3.9 ± 1.9% SD). Because TREM2/DAP12 signaling is known to induce extracellular signal-ing-regulated kinases (ERK) phosphorylation in immature dendritic

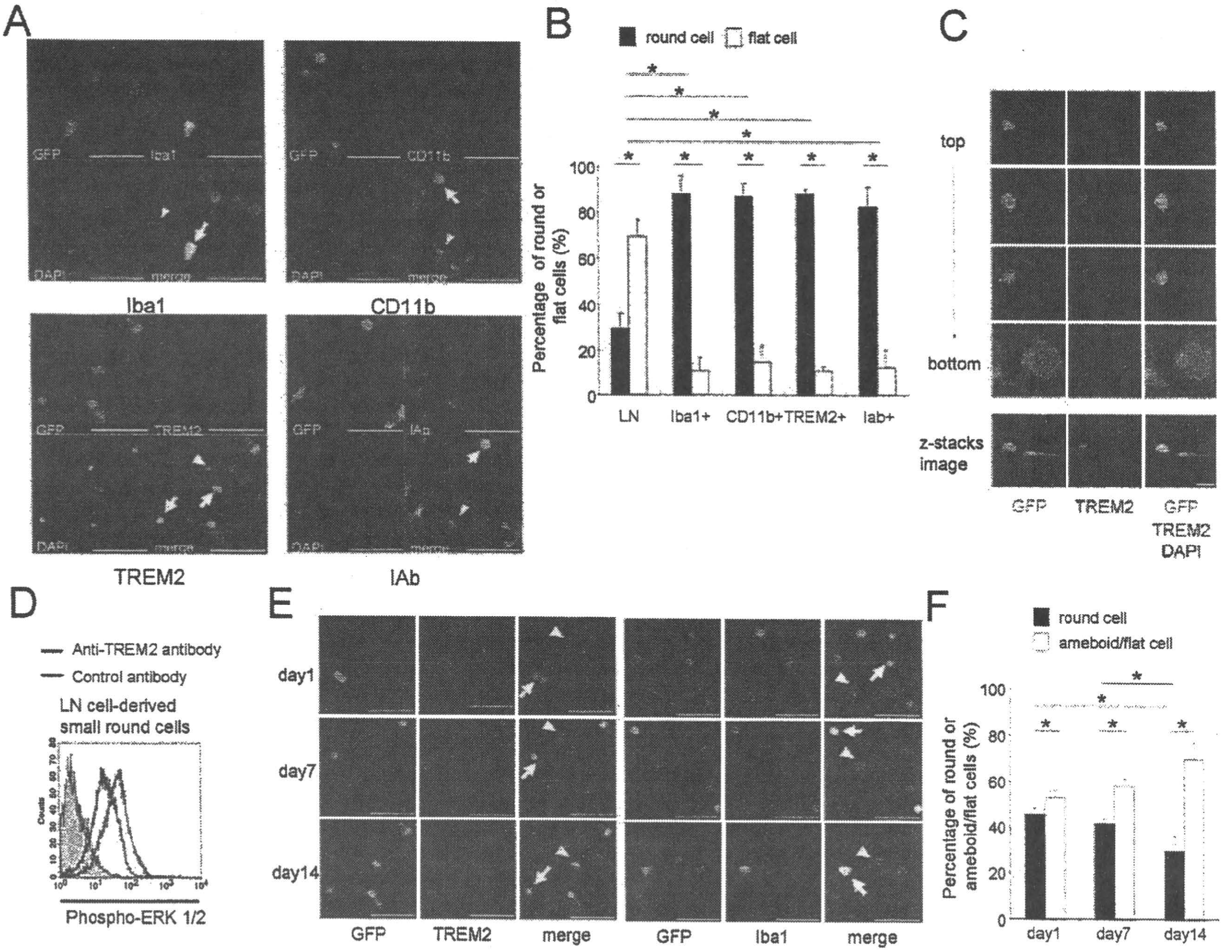

FIG. 3. Lineage-negative bone marrow (LN) cells co-cultured with primary mixed glial culture. (A) Immunocytology of LN cells derived from green fluorescence protein (GFP) mice co-cultured with primary mixed glial culture. Cultures were stained with primary anti-Iba1, anti-triggering receptor expressing on myeloid cells-2 (TREM2), anti-IAb and anti-CD11b antibodies followed by rhodamine- or Cy3-conjugated secondary antibody and 4′,6-diamidino-2-phenylindole (DAPI). Arrows indicate double-positive cells. White arrowheads indicate GFP-negative rhodamine- or Cy3-positive cells. Red arrowheads indicate GFP-positive (GFP+) rhodamine- or Cy3-negative cells. Scale bar: 50 μm. (B) Percentage of round or flat cells among GFP+ cells or double-positive cells. Data are presented as mean ± SD. (C) Z-stack immunofluorescence confocal microscopy of LN cells derived from GFP mice co-cultured with primary mixed glial culture stained with anti-TREM2 (red) and DAPI (blue). GFP and TREM2 double-positive cells show a spherical shape. Scale bar: 10 μm. (D) Phosphorylation of ERK after cross-linking stimulation of LN cell-derived small round cells by flow cytometry. Red line histograms, stimulated with anti-TREM2 antibody; blue line histograms, stimulated with control antibody; filled histograms, stained with isotype-matched control antibody. Data are representative of three independent experiments. (E) Immunocytology of LN cells derived from GFP mice co-cultured with primary mixed glial culture. Cells were fixed at Days 1, 7 and 14 after co-culture and stained with primary anti-TREM2 or anti-Iba1 antibodies followed by rhodamine-conjugated secondary antibody and DAPI. Arrows indicate GFP and TREM2/Iba1 double-positive cells. Arrowheads indicate GFP+ and rhodamine-negative cells. Scale bar: 50 μm. (F) The percentage of round or amoeboid/flat cells among GFP+ cells was quantified by microscopic analysis. The proportion of small round and amoeboid/flat cells of GFP+ cells showed no changes at Days 1 and 7, but the number of small round cells reduced at Day 14. Data are presented as mean ± SD; *$P \leq 0.05$. Data are representative of three independent experiments.

cells, we analysed the phosphorylation of ERK using flow cytometry after cross-linking stimulation of LN cell-derived small round cells in order to determine whether the TREM2 on small round cells was functional. Stimulation of TREM2 of the LN cell-derived small round cells induced phosphorylation of ERK as demonstrated by a specific antibody recognizing the phosphorylated form of ERK (Fig. 3D).

In the kinetic study, GFP+ LN cells were immunostained Days 1, 7 and 14 after co-culturing with primary mixed glial cells with anti-TREM2 and anti-Iba1 antibodies followed by secondary antibodies. At Day 1, LN cells had already differentiated into two morphological groups – small round cells expressing Iba1 and TREM2, and flat amoeboid cells (Fig. 3E). Interestingly, the ratio of LN cell-derived small round and flat cells remained identical at Days 1 and 7, but reduced at Day 14 (Day 1, 45.7 ± 2.5% SD; Day 7, 41.7 ± 1.9% SD vs. Day 1, $P = 0.0495$; Day 14, 29.5 ± 6.4% SD vs. Day 1, $P = 0.0495$; Fig. 3F).

Analysis of surface cell markers and proliferative capacity of LN cell-derived small round cells

In many publications, not only the expression of CD11b, Iba1 and F4/80, but also low expressions of CD45 and MHC class II have been used as microglial markers. Among them, low expressions of CD45 and MHC class II are one of the most important resting microglial markers. We measured the quantitative expression of CD45 and MHC class II on brain microglia, cultured microglia and LN cell-derived small round cells. As shown in Fig. 4A, LN cell-derived small round cells showed low expressions of CD45 and MHC class II, which was identical to results for cultured and brain microglia as compared with those for spleen-derived macrophages. LN cell-derived small round cells were also F4/80 positive, which is known to be another microglial marker.

Because microglia can continue to proliferate and differentiate to macrophages, we investigated the proliferative capacity of brain microglia and LN cell-derived small round cells with various concentrations of M-CSF, and compared this capacity to that of splenic macrophages. LN cell-derived small round cells showed increased incorporation of [^{3}H] thymidine similar to that by brain microglia, but [^{3}H] thymidine incorporation by splenic macrophages did not increase in a low concentration of M-CSF (1 ng/mL; LN cell-derived small round cells vs. splenic macrophages, $P = 0.0495$; brain microglia vs. splenic macrophages, $P = 0.0495$; Fig. 4B).

These results indicate that small round cells and microglia are similar in terms of their cell surface molecules and the proliferative capacity.

Proliferation and differentiation of LN cells in the presence of M-CSF

To examine the humoral factors necessary for the differentiation of LN cells into microglia, we cultured LN cells with the supernatant of the primary mixed glial culture for 7 days. Most of the LN cells cultured with this supernatant (LN-Sup cells) were flat in shape and expressed CD11b, Iba1, TREM2 and IAb (Fig. 5A).

Next, we measured the concentrations of cytokines in the supernatant of the primary mixed glial culture using the Bio-Plex Cytokine Assay System. Among the assayed cytokines, the concen-

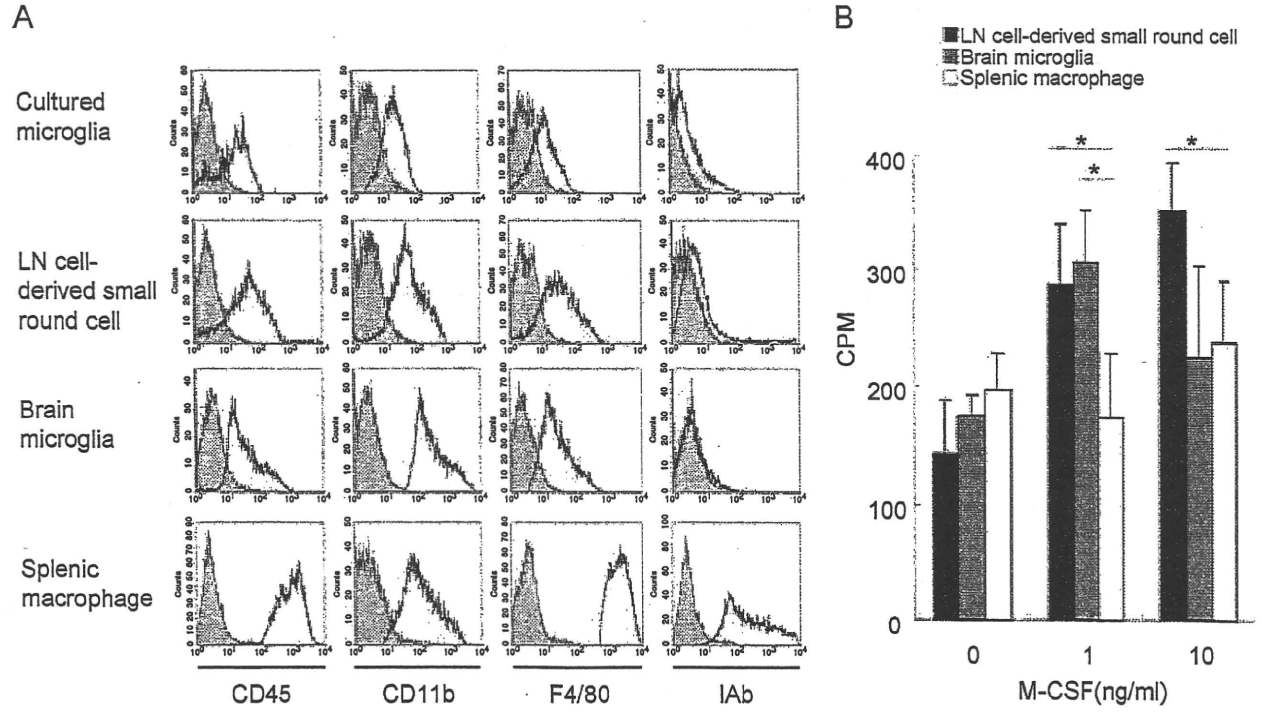

FIG. 4. Surface cell markers and proliferative capacity of lineage-negative bone marrow (LN) cell-derived small round cells. (A) Flow cytometry analysis of cultured microglia, LN cell-derived small round cells, brain microglia and splenic macrophages. Open histograms, staining with antibodies to markers below plots; filled histograms, isotype-matched control antibody. Data are representative of three independent experiments. (B) Proliferative capacity of cultured microglia, LN cell-derived small round cells, brain microglia and splenic macrophages. Proliferation was measured by thymidine incorporation. Data are presented as mean ± SD; *$P \leq 0.05$. Data are representative of three independent experiments. M-CSF, macrophage colony stimulating factor.

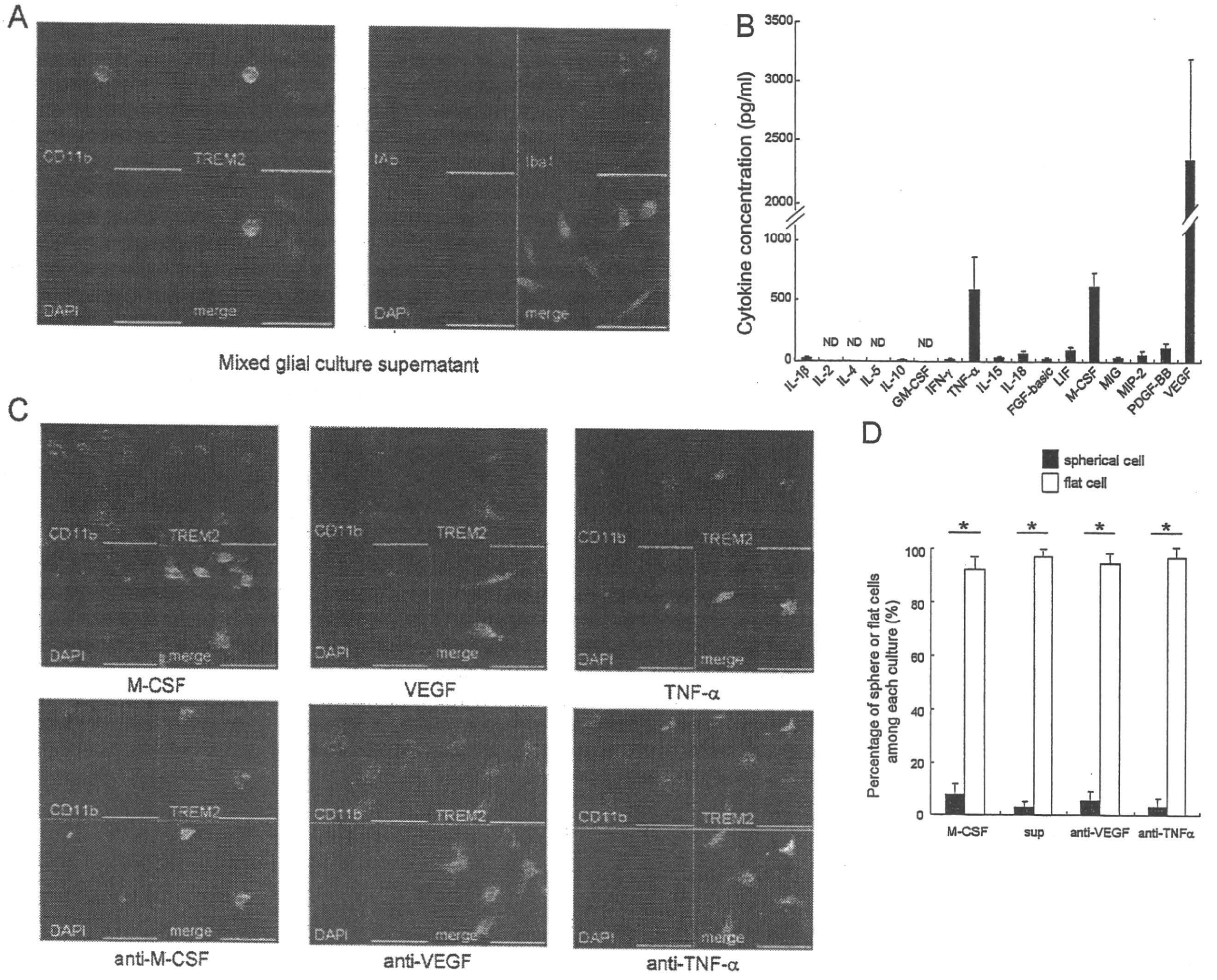

FIG. 5. Proliferation and expression of triggering receptor expressing on myeloid cells-2 (TREM2) on LN cells in the presence of macrophage colony stimulating factor (M-CSF). (A) Immunocytology of LN cells cultured with supernatant of primary mixed glial culture. Cultures were stained with anti-Iba1, anti-TREM2, anti-IAb, anti-CD11b and 4′,6-diamidino-2-phenylindole (DAPI). Scale bar: 50 μm. (B) Analysis of concentration of cytokines [IL-1b, IL-2, IL-4, IL-5, IL-10, GM-CSF, IFN-γ, tumor necrosis factor-α (TNF-α), IL-15, IL-18, FGF-basic, LIF, M-CSF, MIG, MIP-2, PDGF-BB and vascular endothelial growth factor (VEGF)] in the supernatant of primary mixed glial culture by using the Bio-Plex Cytokine Assay System. ND; not detectable. Data are presented as mean ± SD of 12 independent experiments. (C) Immunocytology of LN cells cultured with M-CSF-, VEGF- or TNF-α-containing medium, and anti-MCSF, anti-VEGF or anti TNF-α antibody-containing supernatant of mixed glial culture. The cells were stained with anti-TREM2 antibodies, CD11b antibodies and DAPI. LN cells cultured with M-CSF showed no change in their morphology or surface markers as compared with LN cells cultured with the supernatant of primary mixed glial culture; however, the addition of anti-M-CSF antibodies remarkably reduced the cell number. Scale bar: 50 μm. (D) The percentage of spherical or flat cells was quantified by confocal microscopy. Data are presented as mean ± SD; $*P \leq 0.05$. Data are representative of three independent experiments.

trations of M-CSF, VEGF and TNF-α were remarkably high (614.2 ± 121.5 SD pg/mL of M-CSF, 2349.4 ± 845.9 SD pg/mL of VEGF and 585.5 ± 278.2 SD pg/mL of TNF-α) compared with those of the other cytokines (Fig. 5B). IL-2, IL-4, IL-5 and GM-CSF were not detected, and the concentrations of IL-1β, IL-10, IFN-γ, IL-15, FGF-basic and MIG were very low (24.8 ± 10.7 SD pg/mL of IL-1β, 12.4 ± 6.9 SD pg/mL of IL-10, 18.0 ± 13.0 SD pg/mL of IFN-γ, 34.4 ± 12.5 SD pg/mL of IL-15 and 21.6 ± 11.9 SD pg/mL of FGF-basic). The concentrations of IL-18, LIF, MIP-2 and PDGF-BB were at an intermediate level (61.9 ± 23.3 SD pg/mL of IL-18, 92.5 ± 23.8 SD pg/mL of LIF, 34.7 ± 11.6 SD pg/mL of MIG, 57.0 ± 31.6 SD pg/mL of MIP-2 and 115.7 ± 36.1 SD pg/mL of PDGF-BB).

To investigate the effect of each cytokine on the differentiation of LN cells, we cultured LN cells with M-CSF, VEGF or TNF-α for 7 days. All the LN cells cultured with M-CSF (LN–MCSF cells) were CD11b- and TREM2-positive (Fig. 5C). Morphologically, most LN–MCSF cells showed flat shapes on confocal microscopy (Fig. 5D). The number of LN cells cultured with TNF-α (LN–TNF cells) or with VEGF (LN–VEGF cells) were very few, although these cells expressed CD11b and TREM2 (Fig. 5C).

Next, LN cells were cultured with the mixed glial culture supernatant containing neutralizing antibodies of M-CSF, TNF-α or VEGF. Addition of the anti-VEGF antibody or anti-TNF-α antibody resulted in no change in the morphology or surface markers as compared with the culture containing the control antibodies; however, the addition of anti-M-CSF antibodies remarkably reduced the cell number despite the expression of TREM2 (Fig. 5C).

Cell-to-cell contact between microglia and astrocytes

In order to reveal the role of cell-to-cell contact between microglia and other glial cells, especially astrocytes, in the differentiation of LN cells to microglia, we performed immunostaining of the mixed glial culture with LN cells by anti-GFAP antibody followed by secondary rhodamine-conjugated antibody against rabbit-IgG. Analysis by confocal microscopy revealed that LN cell-derived small round cells were positioned above the GFAP-positive astrocytes (Fig. 6). On the other hand, large flat cells lay immediately beneath the GFAP-positive astrocytes.

Discussion

Microglia, the immune cells of the CNS, exist in three distinct forms – amoeboid, ramified and reactive microglia. Ramified microglia are present in the brain parenchyma and constitute approximately 10–20% of the total population of glial cells in an adult (Vaughan & Peters, 1974; Banati, 2003). Ramified microglia are small round cells comprising branching processes and are considered to be functionally inactive. Further, they are known to express TREM2 *in vivo* (Schmid *et al.*, 2002; Sessa *et al.*, 2004), but not MHC class II (Santambrogio *et al.*, 2001; Servet-Delprat *et al.*, 2002). Recently, HSP60 has been identified as the ligand of TREM2, and its interaction with microglia has been demonstrated to stimulate microglial phagocytosis (Stefano *et al.*, 2009). This result indicates that TREM2 might play an important role in physiological phagocytosis as one of the microglia-specific functions. TREM2 expression on small round cells in primary mixed glial culture might indicate that small round cells have greater mobility as microglia than do large flat cells in patrolling the brain environment in order to identify HSP60-expressing cells. Moreover, as shown in Fig. 4A, small round cells weakly expressed MHC class II molecules similar to brain microglia. These results support our hypothesis that small round microglia *in vitro* differentiated to a greater extent than did large flat cells. Consistent with the results of the current study, previous studies have reported two different morphological shapes of microglia in primary mixed glial culture cells derived from mice (Saura *et al.*, 2003) and rats (Tanaka *et al.*, 1999; Kuwabara *et al.*, 2003). In another study, the kinetic analysis of rat primary mixed glial culture demonstrated that 'amoeboid' or 'round' cells appeared during the early stages of the culture, and that the majority of ramified microglia were formed after the complete formation of the astrocyte monolayer (Tanaka *et al.*, 1999). We demonstrated that LN cells directly differentiated into small round microglia-like cells without the intermediary formation of large flat precursors. Although Ly-6C^{high} Gr-1+CCR2+ monocytes in the peripheral blood have been reported to be the precursors of adult murine microglia (Mildner *et al.*, 2007; Getts *et al.*, 2008), the LN cells in our study did not express CCR2 or Gr-1 (the anti-Gr-1 antibodies used in this study also reacted with Ly-6C). The role of CCR2, a crucial chemokine receptor for the chemotactic attraction of monocytes or macrophages during CNS inflammation, has been investigated in animal models of multiple sclerosis, such as experimental autoimmune encephalomyelitis (Fife *et al.*, 2000; Izikson *et al.*, 2000). However, the physiological development and functions of microglia are independent of CCR2 expression (Mildner *et al.*, 2007). Because the absence of CCR2 expression is highly related to the Ly-6C^{high} subpopulation (Mildner *et al.*, 2007), Ly-6C may play a more important role than CCR2 in microglial differentiation. It is unclear why the LN cells differentiated into small round microglia-like cells despite the lack of Ly-6C and Gr-1 expression, but we hypothesize that the blood–brain barrier plays a key role in the differentiation of LN cells. Indeed, Ly-6C is known to regulate endothelial adhesion and the homing of CD8+T cells by activating integrin-dependent adhesion pathways (Hänninen *et al.*, 1997).

On the other hand, the LN cells in the current study did not differentiate into flat cells as the precursors of small round microglia. Since they were first described by del Rio-Hortega (1932), the developmental origin of microglia has not been completely elucidated. It is widely hypothesized that microglia are derived from myeloid lineage precursors and/or hematopoietic precursors during CNS development. The fact that the formation of microglia occurs before the onset of vascularization in the developing brain (Wang *et al.*, 1996) suggests that hematopoietic stem cells, which act as precursors to microglia during development, may be more primitive than precursor LN cells. Therefore, it is likely that the LN cells adopt a different pathway to differentiate into small round microglia-like cells.

The supernatant of the primary mixed glial cultures derived from mice contains many cytokines, such as M-CSF, VEGF and TNF-α. Our study showed that M-CSF plays an important role in the

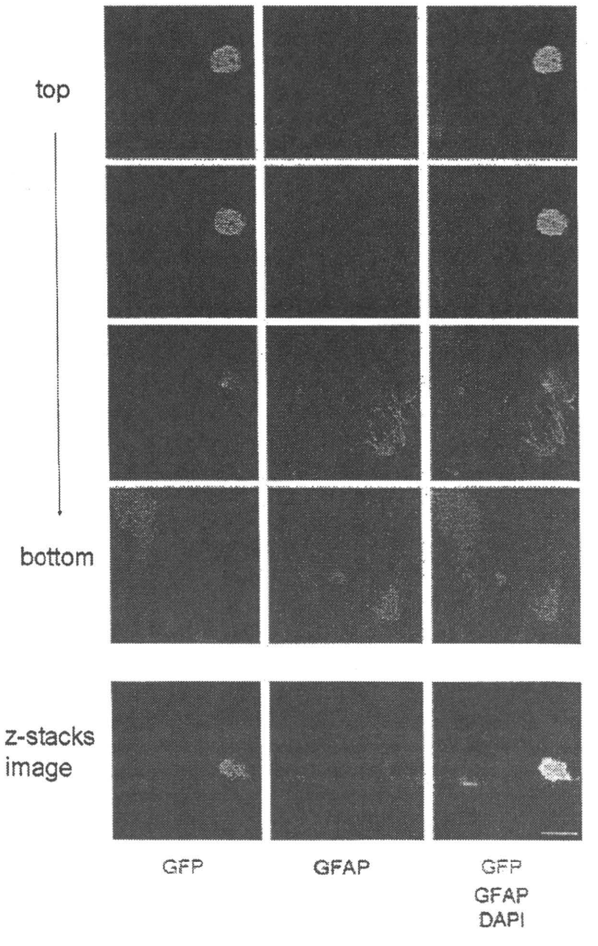

FIG. 6. *Z*-stack immunofluorescence confocal microscopy of LN cells derived from green fluorescence protein (GFP) mice co-cultured with primary mixed glial culture stained with anti-glial fibrillary acidic protein (GFAP; red) and 4′,6-diamidino-2-phenylindole (DAPI; blue). Scale bar: 10 μm.